Evidence of early bottom water current flow after the Messinian Salinity Crisis in the Gulf of Cadiz

Marlies van der Schee*[(1)], F.J. Sierro[(1)], F.J. Jiménez-Espejo[(2)], F.J. Hernández-Molina[(3)], R. Flecker[(4)], J.A. Flores[(1)], G. Acton[(5)], M. Gutjahr[(6)], P. Grunert[(7)], Á. García-Gallardo[(7)], N. Andersen[(8)].

[(1)] *Dept. de Geología, University of Salamanca, Plaza de los Caídos s/n, 37008, Salamanca, Spain*

[(2)] *Dept. of Biogeosciences, JAMSTEC, Yokosuka 237-0061, Japan*

[(3)] *Dept. Earth Sciences, Royal Holloway Univ. London, Egham, Surrey TW20 0EX, UK*

[(4)] *BRIDGE, School of Geographical Sciences, Cabot Institute, University of Bristol, University Road, Bristol, BS8 1SS, UK*

[(5)] *Dept. Geography and Geology, Sam Houston State University, Huntsville, Texas, USA 77341-2148*

[(6)] *GEOMAR Helmholtz Centre for Ocean Research Kiel, Wischhofstr. 1-3, D-24148, Kiel, Germany*

[(7)] *Inst. für Erdwissenschaften, Karl-Franzens-Universität Graz, NAWI-Graz, Heinrichstrasse 26, 8010 Graz, Austria*

[(8)] *Leibniz-Laboratory for Radiometric Dating and Isotope Research, Christian-Albrechts-Universität Kiel, Max-Eyth-Str. 11-13, 24118 Kiel, Germany*

* Corresponding author: Marliesvanderschee@usal.es

Keywords: Miocene-Pliocene boundary; Gulf of Cadiz; IODP Expedition 339; Mediterranean Outflow Water; Messinian Salinity Crisis; Contourites

Abstract

Integrated Ocean Drilling Program (IODP) Expedition 339 cored multiple sites in the Gulf of Cadiz in order to study contourite deposition resulting from Mediterranean Outflow water (MOW). One hole, U1387C, was cored to a depth of 865.6 meters below seafloor (mbsf) with the goal of recovering the Latest Miocene to Pliocene transition in order to evaluate the history of MOW immediately after the end of the Messinian Salinity Crisis. To understand this history, an accurate age model for the succession is needed, but is challenging to construct, because the Miocene-Pliocene boundary is not marked by a clear biostratigraphic event in the Atlantic and coring gaps occur within the recovered stratigraphic record. These limitations are overcome by combining a

variety of chronostratigraphic datasets to construct an age-model that fits the currently available age indicators and demonstrates that coring in Hole U1387C did indeed recover the Miocene-Pliocene boundary at around 826 mbsf. This boundary is associated with a distinct and abrupt change in depositional environment. During the latest Messinian, hemipelagic sediments exhibiting precession-induced climate variability were deposited. These are overlain by Pliocene sediments deposited at a much higher sedimentation rate, with much higher and more variable XRF-scanning Zr/Al ratios than the underlying sediment, and that show evidence of winnowing, particle sorting and increasing grain size, which we interpret to be related to the increasing flow of MOW. Pliocene sedimentary cyclicity is clearly visible in both the benthic $\delta^{18}O$ record and the Zr/Al data and is probably also precessionally controlled. Two contouritic bigradational sandy-beds are revealed above the third sedimentary cycle of the Pliocene. On the basis of these results, we conclude that sedimentation associated with weak Mediterranean-Atlantic exchange, began in the Gulf of Cadiz virtually at or shortly after the Miocene-Pliocene boundary.

1. Introduction

Today, Mediterranean Outflow water (MOW) is the dominant intermediate water mass in the Gulf of Cadiz (Hernández-Molina et al., 2014a). The mixture of relatively warm and saline Mediterranean water and colder, less saline Eastern North Atlantic Central Water (ENACW) proceeds north and north-westwards along the middle slope of the Algarve Margin (Fig. 1; Hernández-Molina et al., 2003a) and preconditions Atlantic Meridional Overturning Circulation, hence also influencing global climate (Ivanovic et al., 2014; Rogerson et al., 2012a).

The present day gateway configuration through the Gibraltar Strait dates back to the astronomically dated Miocene-Pliocene boundary (5.332 Ma; e.g. Lourens et al., 1996; Van Couvering et al., 2000; Blanc, 2002; Duggen et al., 2003; Roveri et al., 2014). Before this, Atlantic-Mediterranean seawater exchange took place through two marine connections, the Betic Corridor in southern Spain and the Rifian Corridor in north west Morocco (e.g. Benson et al., 1991; Santisteban and Taberner, 1983). Exchange became progressively restricted during the Late Miocene as a result of a complex combination of tectonic and relative sea-level processes until the two water bodies became almost completely disconnected (Krijgsman et al., 1999; Kuroda et al., 2016; Lofi et al., 2005; Meijer and Krijgsman, 2005; Ohneiser et al., 2015; Simon and Meijer, 2015). Between 5.97 and 5.33 Ma, the chemical composition and salinity of Mediterranean water must have changed dramatically and thick evaporites precipitated during an extraordinary event known as the Messinian Salinity Crisis (MSC; e.g. Hsu et al., 1973). Immediately after the Messinian, it is thought that physically the Mediterranean and the Atlantic were reconnected through the single gateway. However, the nature of the initial early Pliocene Atlantic-Mediterranean water mass exchange is still unclear (Hernández-Molina et al., 2014a).

Analyses of benthic foraminifera assemblages indicate that water from the Atlantic Ocean penetrated the Eastern Mediterranean within a few precession cycles of the Miocene-Pliocene boundary (Iaccarino et al., 1999a). This, combined with the transition back to normal marine salinities in the Mediterranean, suggests that exchange between the two water bodies took place through the gateway immediately after the Miocene-Pliocene boundary. Seismic reflection profiles, however, are interpreted to indicate that contourites associated with the earliest active bottom water current along the pathway of the present day MOW were deposited significantly later at 4.2-4.5 Ma (Expedition 339 Scientists, 2013a, 2012; Hernández-Molina et al., 2014b). The question is whether any record of early Pliocene MOW prior to 4.2-4.5 Ma can be identified. Possible reasons for the absence of a clear early Pliocene record of MOW include the lack of appropriately located, well-dated sedimentary archives or that the MOW and NACW are too similar to distinguish from each other (Rogerson et al., 2012b).

Integrated Ocean Drilling Program (IODP) Expedition 339 cored Hole U1387C (Fig. 1) in order to recover the first Late Miocene-Pliocene sediment record in the Gulf of Cadiz and to evaluate the re-establishment of Mediterranean-Atlantic exchange after the MSC (Stow et al., 2011). Unfortunately, the Miocene-Pliocene boundary is not easy to identify in the Gulf of Cadiz, since its global stratotype has been established in the Mediterranean where it is associated with the facies shift from Messinian evaporites to Zanclean marls (Van Couvering et al., 2000). Consequently, the Miocene-Pliocene boundary outside the Mediterranean Basin can only be identified using alternative chronostratigraphic methods.

Analyses to detect bottom water currents, for example of Mediterranean-Atlantic exchange, are increasingly done by analysing XRF-core scanning Zr/Al levels in combination with grain size analysis (Bahr et al., 2015; Kaboth et al., 2015; Lamy et al., 2015; Voelker et al., 2015b). In cases where Zr is associated with coarser grain sizes in marine environments, such as in the Gulf of Cadiz, it becomes a typical indicator for sediments affected

by changes in bottom water current strength (Bahr et al., 2014; Bertrand et al., 2012; Ganeshram et al., 1999). The element Zr is most often associated with the dense refractory mineral zircon (e.g. McLennan et al., 1993). Zr/Al peaks are associated with higher proportions of non-aluminosilicate minerals, such as quartz, feldspars, and heavy minerals (zircon). Lower Zr/Al ratios are linked to finer grained Al-rich minerals, such as clays. Bottom water current sorting promotes the separation between coarser siliciclastic sediment components, enrich in Zr, and Al-rich finer grained minerals. For example, Bahr et al. (2014) showed that Latest Pleistocene (0-140 ka) contourites at Site U1387 exhibited high Zr/Al ratios in sandy intervals, which were deposited under high bottom water current flow conditions. By contrast, Zr/Al levels in the hemipelagic core MD01-2444 (Fig. 1) are dominated by long-term variability and shows only small-scale oscillations.

In this study, we establish a refined chronostratigraphic framework for upper Miocene to lower Pliocene sediments recovered at IODP Site U1387 based on seismic correlation, biostratigraphic constrains (planktic foraminifera, calcareous nannofossils), magnetostratigraphy and cyclostratigraphy. We then evaluate the imprint of bottom water currents on the Gulf of Cadiz sediments spanning the Miocene-Pliocene transition using lithology, grain size fractions (>63 μm) and elemental XRF Zr/Al ratios. Our key aim is to identify deposits characteristic for elevated bottom water currents, to evaluate current strength, and if possible to date the onset of post MSC MOW.

2. Background

IODP Site U1387 is located on the continental margin of the Iberian Peninsula at the eastern end of the Faro Drift (36°48´N, 7°43´W) at 559 m water depth (Fig. 1; Expedition 339 Scientists, 2013a, 2012).This study focuses on the lowermost section of Hole U1387C from 731.2 mbsf to the bottom of the sediment sequence at 865.6 mbsf. These are the oldest sediments recovered during the IODP Expedition 339. Core recovery over this interval was 64% and downhole logging data was not collected because of borehole wall collapse, which means that the record contains significant gaps.

Using the Last Occurrence (LO) of *Globorotalia margaritae* (3.85 Ma; Hilgen et al., 2012) at 560.4 mbsf, the First Occurrence (FO) of *Globorotalia puncticulata* (4.52 Ma; Lourens et al., 2004) at 630.82 mbsf in combination with the presence of *G. margaritae* at the bottom of the core (younger than 6.35 Ma; Hilgen et al., 2012; Table 1) and the absence of *Globorotalia miotumida*, shipboard scientists suggested that sediments from 731.2-865.6 mbsf were Miocene/Pliocene in age (Expedition 339 Scientists, 2012; Stow et al., 2013a; Hernández-Molina et al., 2014). However, there is no robust justification of the depth for the Miocene-Pliocene boundary due to limited tie point identifications during the Expedition (Expedition 339 Scientists, 2013a, 2012). Although the exact depth of the boundary is never clearly stated in any of these publications, it is apparent from the various stratigraphic summary figures that so far the boundary was poorly constrained. The preferred depth of ~730 mbsf used in the summary by Hernández-Molina et al. (2014a) centered on IODP Expedition 339 results was based on a lithologic transition from hemipelagites of presumed Miocene age to turbidites and debrites of presumed Pliocene age. However, the ~730 mbsf estimate was clearly not a precise depth for the Miocene-Pliocene boundary.

Recently, 3D and 2D seismic reflection profiles have been used to correlate the Algarve-2 well to IODP Site U1387 (Figure 1, Hernández-Molina et al., 2015). The Miocene-Pliocene boundary in Algarve-2 has been identified at 1455-1460 mbsf using a combination of biostratigraphic data and

cyclostratigraphic tuning of resistivity logs (Hernández-Molina et al., 2015). The Miocene-Pliocene boundary is manifested as an increase in reflection amplitudes on seismic lines (M-reflector) truncating towards the basin margins. This reflector was correlated by Hernández-Molina et al., (2015) to an abrupt sedimentary change in Site U1387 at ~826 mbsf with an uncertainty of 15-20 m.

Core descriptions prepared during IODP Expedition 339 describe the lithology between 731.2-751 mbsf as greenish grey to very dark greenish grey nannofossil (silty) mud or sand with biogenic carbonate (Fig. 2A; Expedition 339 Scientists, 2013). Shipboard colour reflectance data (L*) mirrors to some extent darker and lighter colours of the sediments (Fig. 2G). Cemented grey medium sandstone with biogenic carbonate is found between 750.39 and 750.92 mbsf (Fig. 2B). From 760 mbsf to the base of the core, dark greenish grey nannofossil mud and muddy/clayey nannofossil ooze is found commonly interbedded with 2 cm thick beds of dark greenish grey silty sand (Fig. 2D). The deepest occurrence of a thick (~80 cm) silty bed is observed at about 801 mbsf (Fig. 2C). Distinct bioturbation is present from 827.2 to 865.2 mbsf (Fig. 2E), but is less extensive higher up the sequence. Hence, compositional lithological changes exist at several depths in the studied section. While the Miocene-Pliocene boundary was previously presumed to be associated with the significant change in lithology at ~730 mbsf (Hernández-Molina et al., 2014b), it was just as likely represented by one of the other notable changes in lithology.

Finally, shallow water benthic foraminifera, such as *Ammonia, Elphidium* and *Asterigerinata* were recorded from 792.8 mbsf upwards and have particular high abundances above 765.72 mbsf (Expedition 339 Scientists, 2013a).

3. Methods

3.1 Sample preparation

Bulk sediment samples from IODP Hole U1387 of ~25 cm^3 were collected at the IODP Bremen Core Repository for micropaleontological, stable isotope, and grain size analyses. Samples were taken every 40 cm from 731 to 748 mbsf and every 20 cm from 750 to 866 mbsf. All samples were freeze-dried overnight, weighed, disaggregated in tap water overnight, sieved through >63 and >150 µm sieves, dried, and weighed again. The >63 µm fraction of the total dry weight was used as the sand fraction, indicative of bottom water currents flow strength (Rogerson et al., 2005).

Paleomagnetic samples consisted of the archive halves of all core sections and oriented discrete sediment samples, which were collected by inserting a hollow extruder into the middle of the working half of the split-core sections and then extruding the sediments into plastic cubes (2 cm × 2 cm × 2 cm, with an internal volume of ~7 cm^3) as described in Expedition 339 Scientists, (2013b).

3.2 Micropaleontological studies

Planktic foraminifera biostratigraphic analyses was performed on the >150 µm fraction of the prepared samples. A microsplitter was used to split residues until about 150 planktic specimens remained. All planktic foraminifera species were counted and classified including the biostratigraphic marker species *G. margaritae*, *Globorotalia menardii* and sinistral or dextral coiling *Neogloboquadrina acostaensis.* Presence/absence data of benthic foraminiferal species on the >150 µm fraction were used to provide a rough paleobathymetry estimation [A detailed quantitative analysis will be available in a separate publication by García-Gallardo et al., in preparation]. Five samples were chosen for detailed calcareous nannofossils biostratigraphic analysis, implementing the settling technique described in Flores and Sierro (1997).

3.3 Stable isotope analyses

Between two and fifteen specimens of the benthic foraminifera *Cibicidoides pachyderma* >250 µm were hand-picked from each sample for carbon and oxygen isotope analysis ($\delta^{13}C$, $\delta^{18}O$). Specimens were washed with ethanol, ultrasonicated for several seconds and dried for 24 hours to remove all liquids.

Samples from 866 to 827 mbsf and 731 to 748 mbsf were analysed in the Godwin Laboratory for Palaeoclimate Research at the University of Cambridge. Isotope analyses were performed using a Thermo Finnigan MAT253 mass spectrometer fitted with a Kiel device. Analytical precision on an in-house standard, calibrated against international carbonate standard NBS-19, is estimated to be ±0.06 ‰ for $\delta^{13}C$ and ±0.08 ‰ for $\delta^{18}O$. Results are reported relative to V-PDB. Samples from 748 mbsf to 827 mbsf were analysed in the Leibniz-Laboratory for Radiometric Dating and Isotope Research at the Christian-Albrechts-University in Kiel with a MAT 253 mass spectrometer connected to a Kiel IV carbonate preparation device. The analytical precision of the NBS-19 international standard and three laboratory-internal standards was better than ±0.05 ‰ ($\delta^{13}C$) and ± 0.08 ‰ ($\delta^{18}O$). Large foraminiferal samples with more than six individuals were crushed to homogenise the samples before analysis of a representative subsample was undertaken.

3.4 X-ray fluorescence analyses

We used the XRF core scanner II, (AVAATECH Serial No. 2) at the MARUM—University of Bremen to retrieve elemental Zr/Al ratios. XRF core scanner data were collected every 3 cm down-core over a 1.2 cm^2 area with a down-core slit size of 10 mm in three separate runs using generator settings of 10, 30, and 50 kV, and currents of 0.2, 1.0, and 1.0 mA, respectively. Sampling time was set to 20 s and scanning took place directly at the split core surface of the archive half. The split core surface was covered with a 4 µm thin SPEXCerti Prep Ultralene1 foil to avoid contamination of the XRF measurement unit and desiccation of the sediment. The reported data have been acquired by a

193 Canberra X-PIPS Silicon Drift Detector (SDD; Model SXD 15C-150-500) with 150 eV X-ray resolution
194 and the Canberra Digital Spectrum Analyzer DAS 1000. The XRF II scanner is equipped with an Oxford
195 Instruments 50W XTF5011. Core disturbance from drilling (biscuiting) may have significantly
196 degraded the quality of XRF-measurements from 760.18 to 764.94 (Core 51R) and inhibited
197 measurements from 816.58 to 827.23 mbsf (Core 57R).

198 ### 3.5 Magnetostratigraphy

199 As described in Expedition 339 Scientists (2013a, b), continuous paleomagnetic measurements were
200 made every 5 cm along the split-core sections during Expedition 339 using the shipboard cryogenic
201 magnetometer (2G Enterprises Model-760R). The natural remanent magnetization (NRM) was
202 measured after progressive alternating field (AF) demagnetization at 0, 10, and 20 mT. The split-
203 core data were further cleaned by removing results from disturbed intervals and from near the ends
204 of the core sections, as these data contain biases. The cleaned data are available in Table T16 of
205 Expedition 339 Scientists (2013a) and the raw data are available online from the IODP LIMS
206 Database.

207 To permit more detail demagnetization experiments and to better assess the characteristic
208 remanent magnetization (ChRM) directions, we also collected approximately one discrete
209 paleomagnetic cube sample (7 cm^3) from each core section (roughly one sample every 1.5 m) during
210 Expedition 339 for the interval from 700 mbsf to the base of the hole, for a total of 56 samples. Only
211 four of these samples were measured during Expedition 339. The remaining 52 were measured post-
212 cruise in the Paleomagnetism Laboratory at University of California-Davis. All 56 samples were
213 subjected to progressive AF demagnetization generally using 5 mT steps from 0 to 40 mT and 10 mT
214 steps up to 100 mT. Paleomagnetic directions were determined from principal component analysis
215 (PCA) (Kirschvink, 1980) using ZPLOTIT software (Acton, 2011,
216 http://paleomag.ucdavis.edu/software-zplotit.html). The remanence measurements from at least

five demagnetization steps for each interval were fit to lines using only steps between 20 and 60 mT. PCA lines were fit using both the FREE option, in which the line is not required to pass through the origin of the plot, and the ANCHORED option, in which line is anchored to the origin (Supplementary Tables S17-S19). A Fisherian mean direction was also computed from the highest several demagnetization steps to estimate a stable end point (SEP). The paleomagnetic data and PCA results are provided in the Supplementary Material.

For each sample, we determined a preferred inclination from the PCA FREE, PCA ANCHORED, or SEP estimate of the ChRM. The selection of which method best resolved the ChRM was based on visual inspection of the sample directions plotted on orthogonal vector diagrams (modified Zijderveld plots) and stereonets. The results for each sample were ranked with a quality factor, where Quality 1 was reserved for samples that displayed very linear decay of magnetization during demagnetization as noted by PCA maximum angular deviation (MAD) angles < 5. Quality 2 are similar to Quality 1 but the MAD angles are between 5° and 10°. These highest quality (1 and 2) samples have very well resolved ChRM directions and the polarity can be determined with great confidence. Such high quality samples occur mainly in the upper part of section, and none are deeper than 550 mbsf. Quality 3 samples displayed moderate directional scatter during AF demagnetization but a relatively noisy ChRM can be determined from which the polarity can be established. Quality 4 samples have large directional scatter during AF demagnetization and generally a significant drilling overprint that overlaps much of the coercivity spectra of the ChRM. The ChRM cannot be accurately determined although it is often possible to determine the polarity of these samples because they trend toward positive (normal polarity) or negative (reverse polarity) inclinations as they are demagnetized above about 40-80 mT. Quality 5 samples have such highly variable directions during AF demagnetization or are so strongly overprinted that their polarity is indeterminate. Of the 56 samples below 700 mbsf, only 3 are Quality 3, 33 are Quality 4, and the remaining 20 are Quality 5.

4. Results

The sedimentary sequence was divided into three intervals based on its lithological and geochemical properties (Fig. 3): Interval I (826 to 865.6 mbsf) is characterised by low Zr/Al levels and consistently low weight % sand; Interval II (826 to 760 mbsf) has higher, more variable Zr/Al ratios and progressively higher and more variable grain size; Interval III (731.2 to 760 mbsf) is characterised by highly variable Zr/Al oscillations and much higher weight % sand commonly reaching 10-40 weight %.

4.1 Sand fraction and composition

The sand fraction >63 µm of Interval I is consistently less than 3 weight % (Fig. 3). Microscopic inspection of washed samples revealed that this coarser fraction mainly consists of planktic foraminifera with minor lithic particles including pyrite and rare quartz. A similar grain size and composition is observed in the lower part of Interval II (Cores 56R and 57R), but samples with distinctly higher contents of >63µm fraction occur increasingly commonly above 803 mbsf. The coarser grain size is associated with an increase in the quartz content. Sediments in Cores 53R and 54R show distinct bigradational grain size patterns with traces of bioturbation (Fig. 2D, 4). The sand fraction of these silt horizons is dominated by fine sand-grade material (e.g. between 63 and 150 µm; Fig. 4). The composition of the >150 µm fraction is mainly restricted to foraminifera and peaks in the abundance of this coarser size fraction show no relationship with the bigradational pattern seen in the fine-sand material (Fig. 4). The higher sand content seen in Interval III is associated with more lithic particles, mainly quartz grains (Fig. 3).

4.2 Stable isotope records

The benthic $\delta^{18}O$ isotope record shows regular fluctuations throughout the studied section. However, the different intervals are characterised by variations with different wavelengths and amplitudes (Fig. 3). The $\delta^{18}O$ oscillations in Interval I have an average wavelength of ~2.2 m,

considering an additional fourth alternation in Core 61R that is only visible in the $\delta^{13}C$ during the larger $\delta^{18}O$ oscillation from 856.68 to 860.48 mbsf (Table 2; Fig. 3, 9). [A detailed interpretation of the $\delta^{13}C$ record is beyond the scope of this paper and is the subject of a forthcoming paper (Van der Schee et al. in preparation)]. The regular $\delta^{18}O$ alternations in Interval II typically have significantly longer wavelengths of ~6 m on average. Limited recovery of Interval III makes the wavelength of its $\delta^{18}O$ alternations more difficult to calculate, but it appears to be comparable to those of Interval II. The average $\delta^{18}O$ in Interval III is lower than in Intervals I and II (Fig. 3). In all three intervals, distinctly darker layers tend to be associated with higher $\delta^{18}O$ (Fig. 3).

4.3 XRF-scanning Zr/Al ratios

Zr/Al ratios in Interval I have consistently low ratios with the lack of obvious cycles that resemble the periodicity of those well developed in the $\delta^{18}O$ for this interval (Fig. 3A, B). By contrast, Intervals II and III are characterized by distinct, high amplitude variability in the Zr/Al levels displaying cycles with wavelengths similar to those of the benthic isotope record (~6 m). In general, the two records show negative co-variation (Fig. 3).

4.4 Paleobathymetry estimations from benthic foraminiferal presence/absence data.

Presence/absence data of benthic foraminifera are given in the Supplementary material. The studied samples frequently contain benthic foraminifers known to have their upper limit of bathymetric distribution at upper to middle bathyal water depths (e.g., *Cibicidoides pachyderma*, *Cibicidoides . wuellerstorfi*, *Laticarinina pauperata*, *Eggerella bradyi*, *Epistominella exigua*, *Fissurina* spp., *Gyroidinoides* spp., *Melonis* spp., *Oolina* spp., *Osangularia culter*, *Pullenia* spp., *Saracenaria* spp., *Vulvulina pennatula*; (Jones, 1994; Leckie and Olson, 2003; Van Morkhoven et al., 1986). Furthermore, the assemblages contain many taxa that characterize slope environments between 300 and 900m water depth in the Gulf of Cadiz and the western Iberian Margin (e.g., *Amphicoryna scalaris*, *Bigenerina nodosaria*, *Bulimina striata*, *Cibicidoides mundulus*, *Globocassidulina*

289 *subglobosa*, *Planulina ariminensis*, *Uvigerina mediterranea*, and *U. peregrina*; (Phipps et al., 2012;
290 Schönfeld, 2002, 1997). A particularly interesting species amongst the bathyal taxa is *Laticarinina*
291 *pauperata*, a cosmopolitan species that tolerates a wide range of environmental conditions at
292 bathyal and abyssal water depths (van Morkhoven et al., 1986). While other taxa limited to bathyal
293 water depths occur in Interval I as well as Interval II and III, this species disappears from the record
294 above 826 mbsf. An upper depth limit at the middle/upper bathyal transition has been suggested
295 for *L. pauperata*, and its disappearance may indicate a slight shallowing from middle to upper
296 bathyal water depths comparable to today (van Morkhoven et al., 1986).

297 Foraminiferal species restricted to neritic environments such as *Ammonia* spp., *Asterigerinata* spp.,
298 *Cancris* spp., and *Elphidium* spp. are increasingly present above 801 mbsf (Leckie and Olson, 2003;
299 Mendes et al., 2012). These taxa occur throughout the record alongside bathyal species mentioned
300 above and are thus considered allochthonous.

301 # 5. Chronostratigraphic framework

302 ## 5.1. Bio- and magnetostratigraphy

303 ### *5.1.1 Planktic foraminifera*
304 Several planktic foraminiferal species provide constraints on the age of the basal part of IODP Hole
305 U1387 (Table 1). These include:

306 1. The first occurrence of *Globorotalia puncticulata* (4.52 Ma; Hilgen et al 2012) which has been
307 identified in IODP Hole U1387C at a depth of 630.82 mbsf (Expedition 339 Scientists, 2013a).
308 The interval of interest (731.2 - 865.6 mbsf) is therefore entirely older than 4.52 Ma.
309 2. *Neogloboquadrina acostaensis* which is abundant in late Messinian to early Pliocene sediments
310 from this region and exhibits well-dated changes in predominant coiling direction (Krijgsman et
311 al., 2004; Sierro et al., 2001; Lourens et al., 2004). Typically, assemblages strongly dominated

by sinistral coiling *N. acostaensis* are found in sediments older than 6.37 Ma, while dextral coiling shells constitute the vast majority of specimens in sediments younger than 5.82 Ma (Hilgen and Krijgsman, 1999; Krijgsman et al., 2004; Sierro et al., 2001). Quantitative assessment of the coiling direction of *Neogloboquadrina acostaensis* in the lower part of IODP U1387 shows that it is strongly dominated by dextral coiling forms (Fig. 5). Consequently the base of the hole is most likely younger than 5.82 Ma.

Two dextral to sinistral coiling shifts are found from 808.22 to 809.52 and at 841.8 mbsf (Fig. 5). In the Mediterranean Basin during the Pliocene, two sinistral influxes are reported and astronomically tuned in the Eraclea Minoa section as 5.30 and 5.32 Ma (Lourens et al., 1996). Equivalent influxes to these are described in precession driven Cycle 2 and 3 immediately above the Miocene-Pliocene boundary in ODP holes 974B and 975B (Iaccarino et al., 1999b).

3. A distinct high abundance interval, referred to as "acme", of *Globorotalia margaritae* has been described from several latest Miocene records from the Gulf of Cadiz, SW Spain and NW Morocco (Van de Berg et al., 2015; Krijgsman et al., 2004; Ledesma, 2000; Sierro et al., 1993, 1982). The "acme" has an abundance of *G. margaritae* that exceeds at least 10% of the total planktic foraminifera assemblage (Krijgsman et al., 2004; Ledesma, 2000; Sierro et al., 1993, 1982). An interval of particular high abundance occurs in the Ain el Beida section (> 20 %; NW Morocco; Krijgsman et al., 2004) and the Montemayor core (> 37%; SW Spain; Van den Berg et al., 2015) between respectively, ~5.75-~5.70 Ma and ~5.84 Ma (both sites) where the "acme" coincides with glacial stages TG20 and TG22 (Krijgsman et al., 2004). Foraminiferal counts from the lower part of IODP Hole U1387C show that only one sample contains >10% *G. margaritae* (805.42 mbsf; Fig. 5), indicating that this sedimentary succession does not overlap the very high abundance "acme" identified at ~5.75-~5.70 to ~5.84 Ma. The relative large time-span of the "acme" seems to be too long to coincide within

a coring gap (see section 5.2.2). In addition, it is unlikely that the "acme" would not be present even though the sediments of this time-interval might have been covered, since it has always been found in Gulf of Cadiz sections. Since the coiling direction of *N. acostoensis* indicates that these sediments are most likely younger than 5.82, the *G. margaritae* data further constrains the age of the sediments to being younger than ~5.70-~5.75 Ma. Outside the very high abundance interval, Krijgsman et al. (2004) included all samples with >5 % *G. margaritae* in the wider "acme" interval that spans 5.84 to 5.56 Ma. As our quantitative *G. margaritae* data typically varies between 2 and 10 % (Fig. 5; Supplementary material), it is possible that these sediments at the base of IODP Hole U1387C overlap, at least in part, with the described 5.84 to 5.56 Ma interval.

4. An influx of *G. menardii* with a maximum abundance of 5.5 % is recorded between 752.4 and 751.3 mbsf (Fig. 5; Supplementary material). Three similar influxes have been documented from the latest Messinian and earliest Pliocene in the Ain el Beida and Loulja sections in NW Morocco with astronomical ages of 5.550, 5.511 and 5.319 Ma[1]. Without more robust age constraints the influx of *G. menardii* in IODP Site U1387 cannot be correlated to any of these.

In summary, planktic biostratigraphic results suggest that the interval from 731.2 to 865.6 mbsf is older than 4.52 Ma, the first occurrence of *G. puncticulata* (630.82 mbsf) and younger than the high abundance *G. margaritae* "acme" at 5.75 Ma.

5.1.2 Calcareous nannofossils

Characteristic markers species from the latest Neogene are common with individuals of *Amaurolithus primus, Discoaster surculus, Discoaster pentaradiatus* and *Discoaster quinqueramus* as well as characteristic reticulofernestrids (*Reticulofenestra pseudoumbilicus, Reticulofenestra*

[1] Please note that Krijgsman et al. (2004) incorrectly identify *G. menardii* pulses as *Globorotalia miotumida.* (Tulbure et al., in preparation), while they are referred to as *G. menardii* in van der Laan et al. (2006) (Van den Berg et al., 2015).

358 *minuta, Reticulofenestra minutula* and *Reticulofenstra rotaria*), allowing to place the studied
359 interval between zones NN11 and NN15 spanning from 3.81 - 7.36 Ma (e.g. Young et al., 1994; Raffi
360 et al., 2006). The presence of reworked specimens, mainly of Paleogene and early-middle Miocene
361 age (e.g. *Cyclicargolithus floridanus, Discoaster deflandei, Sphenolithus belemnos* gr., among others)
362 is common (Raffi et al., 2006). Expedition 339 Scientists, (2013a) report the LO of *D. quinqueramus*
363 at 811.43 mbsf that indicates an age younger than 5.54 Ma (Raffi et al., 2006). However, the LO of
364 *D. quinqueramus* is hard to identify in such detail, because only a few specimens of *D. quinqueramus*
365 are present and thus could easily be reworked. Also, a few specimens of *R. rotaria* are found in the
366 studied interval which indicate an age range from 7.0-7.41 Ma (Flores et al., 2005; Raffi et al., 2006;
367 Young et al., 1994). The planktic foraminiferal bio-events are clearly indicating Upper Messinian and
368 not upper Tortonian/lower Messinian as indicated by *R. rotaria.* If *R. rotaria* and planktic
369 foraminifera were in-situ, specimens of *Globorotalia miotumida* and continuous abundances of
370 *Globorotalia menardii 5* were expected (Lourens et al., 2004). The incompatibility of the nannofossil
371 and foraminifera data suggest that the few specimens of *D. quinqueramus* and *R. rotaria* are
372 reworked.

373 ### *5.1.3 Magnetostratigraphy*

374 The paleomagnetic data is generally of low quality because the sediment magnetizations are
375 relatively weak and the magnetization of the cores includes a significant drilling overprint that masks
376 the original depositional magnetization. The overprint has a steep downward direction (positive
377 inclinations) similar to that expected for normal polarity intervals. Hence, failure to remove the
378 drilling overprint with magnetic cleaning, such as AF demagnetization, can bias the magnetic polarity
379 interpretation significantly. This is particularly the case for the split-core sections, which give
380 virtually only positive inclinations even in intervals that must be reverse polarity. The 20-mT peak-
381 field AF demagnetization used during Expedition 339 was clearly insufficient in removing the drilling

overprint and resolving the original depositional magnetization, and thus no polarity could be determined from this data below 500 mbsf.

The discrete samples were subjected to much higher peak-field AF demagnetization, which was successful at removing the drilling overprint from many of the samples from Hole U1387C. Even though the quality of the samples is generally considered poor for resolving the ChRM fully, the polarity of the samples could be reasonably well estimated. This is illustrated in Figure 6 where the inclinations are shown for the interval from 550 mbsf to the base of the hole, along with the interpretation of the magnetozones.

Most importantly for the present study is that the stratigraphic section below 800.65 mbsf is all reversely magnetized. Based on the biostratigraphic constraints, this magnetozone corresponds to Chron C3r (5.235-6.033 Ma; Lourens et al., 2004). The base of this magnetozone was not recovered, which is consistent with the biostratigraphic constraints that suggest the age of the bottom of the hole is <5.75 Ma. The overlying normal polarity magnetozone spanning 743.99-800.65 mbsf corresponds to Chron C3n.4n (4.997-5.235 Ma; Lourens et al., 2004), indicating the boundary between the magnetozones at 800.65 mbsf has an age of 5.235 Ma. The Miocene-Pliocene boundary is thus below 800.65 mbsf and above the base of the Hole (865.6 mbsf). The sequence of magnetozones above Magnetozone C3n.4n fits well the general chron sequence of the geomagnetic polarity timescale and the depths and dates of the observed reversals agree well with biostratigraphic constraints and give sedimentation rates compatible with the other chronostratigraphic constraints (Fig. 7).

5.2 Cyclostratigraphic constraints

5.2.1 Precessionally forced variations

Benthic $\delta^{18}O$ records in open ocean deep marine settings during the Pliocene-Pleistocene are mainly dominated by obliquity. However, the first ~150 ky at the base of the Pliocene show a strong precessional signal in the LR04 stack (Fig. 8B; Lisiecki and Raymo, 2005). In contrast, rhythmic sedimentary cycles, including resistivity, gamma ray and Ti/Al records from the Iberian and Moroccan Atlantic margins during the Messinian and Early Pliocene typically display a pronounced variability in response to precession (e.g. Hodell et al., 1994; Krijgsman et al., 2004; Pérez-Asensio et al., 2014, 2013; van der Laan et al., 2012, 2006, 2005; van den Berg et al., 2015). Precession continues to be dominant as astronomical forcing in all IODP sites drilled in the Gulf of Cadiz throughout the Pleistocene, including Site U1387 (Bahr et al., 2015; Lofi et al., 2015; Voelker et al., 2015b).

Precession and obliquity patterns are further investigated by comparing the $\delta^{18}O$ from Loulja with obliquity and a combined record of normalized Precession and negative Tilt (obliquity), hereafter Precession-Tilt (Fig. 8A, 8B). Obliquity is expressed in Precession-Tilt by the enhancement of the amplitude of every other precession cycle. This distinct pattern is clearly visible in Loulja, for example around interglacial stage TG9 (5.45 Ma; Van der Laan et al., 2006). Here, the expression of TG9 is more pronounced due to increased influence of obliquity, while the precession cycles before and after TG9 have lower amplitudes.

The discontinuous nature of the record in the studied interval of Hole U1387C makes it impossible to assess the cyclic patterns in the same way as can be achieved for continuous successions. However, in Interval I, a few continuous regular alternations are visible mainly in the $\delta^{18}O$. Benthic $\delta^{18}O$ cyclical patterns in Cores 61R, 59R and 58R, show alternations of high and low amplitude oscillations (Fig. 9), that are very similar to the typical interference patterns of obliquity and

precession. To illustrate this, we show a comparison of the benthic $\delta^{18}O$ with a theoretical cyclic obliquity and precession pattern (Fig. 9). A similar, close relationship between the $\delta^{18}O$ benthic record and the Precession-Tilt curve is seen as in the Loulja section for the upper Messinian (Fig. 8A, 8B).

In even more detail, Core 61R reveals three full regular alternations in the $\delta^{18}O$-record, while the $\delta^{13}C$ from the same foraminifera specimens shows four regular alternations (Fig. 3, 9). Ventilation patterns and organic carbon storage normally explain $\delta^{13}C$ variations. In the Gulf of Cadiz $\delta^{13}C$ variations have been explained as an expression of ventilation patterns linked to MOW during the Pleistocene with a strong precessional component (Voelker et al., 2006, 2015b), however, linking our data with these patterns without a definite understanding of the connection between the Atlantic and Mediterranean is problematic. Independently, other well-dated benthic Messinian-Early Pliocene benthic-$\delta^{13}C$ records in the area possess a precession component, i.e. Ain el Beida and Loulja (Van der Laan et al., 2012, 2006). Consequently, it is likely that the four $\delta^{13}C$ regular alternations represent precession, while the long $\delta^{18}O$ alternation from 856.9 to 860.3 is the expression of diminished precession under a strong influence of obliquity. This suggests that the short scale visible regular alternations in the $\delta^{18}O$-record during Interval I are precession-induced cycles, with influence of other astronomical cyclicities.

Regular alternations have larger wavelengths during Interval II and III, while coring gaps are still present. As a result, comparing cycle patterns as done for Interval I is impossible, because only one or two cycles can be recognized between gaps. We assume that the $\delta^{18}O$ cyclic patterns are representing the same astronomical variations as in Interval I. Consequently, precessionally forced variability is assumed for the colour changes, Zr/Al ratios and, to some extent, grain size analyses that have wavelengths consistent with the benthic $\delta^{18}O$-record.

5.2.2 Depositional time-span

If the cycles in IODP Hole U1387C are precessionally controlled, the depositional time-span can be calculated given that the average duration of a precession cycle is ~21.7 ka (Berger, 1984) and using the same sedimentation rate for intervals where no core was recovered as is measured in the cores below and above. No significant stretching or shortening of the sediment inside the core pipe during drilling is anticipated because the sediment throughout the Hole is well compacted.

In Interval I, Cores 58R, 59R and 61R all show distinct colour and $\delta^{18}O$ cycles with an average wavelength of 2.2 m per cycle (Table 2). Assuming this constant sedimentation rate, Interval I (38.68 m) should equate to ~18 precession cycles and a time-span of ~389 ky. The occurrence of two colour cycles and two carbon isotope excursions from 856.9 to 860.3 suggest the presence of two precession cycles during the long $\delta^{18}O$ cycle (Fig. 3, 9).

In Interval II, the cores with more continuous recovery (Cores 57R to 54R) show an average thickness of 5.89 m per cycle (Table 2). Interval III appears too short to calculate an individual sedimentation rate in the same way, but it is clear that Core 48R has one long $\delta^{18}O$-variation with a width of 5.71 m, which is presumably representing nearly a full cycle. Uncertainty increases due to a possible additional, subtly expressed cycle in Core 48R, as is hinted in the Zr/Al oscillations. However, this still suggests that the sedimentation rate throughout Interval II and III remains relatively constant. Thus, the total thickness of Interval II and III (97.72 m) equates to ~16 precession cycles, with an average sedimentation rate of about 27.2 cm/ka and a total depositional time span of ~349 ky.

5.3 Tentative working hypothesis on the age model for IODP U1387C

While individually, none of these different datasets provide robust age constraints, more confidence can be gained if the stratigraphic interpretation is compatible with all of them. Here, we explore the best possible stratigraphic fit between the data available.

Assuming, on the basis of the seismic correlation (Hernández-Molina et al., 2015), that the Miocene-Pliocene boundary occurs at the abrupt lithological change between Interval I and II (826 mbsf), the duration of the ~18 precession cycles (389 ky) in Interval I suggests that the age of the bottom of Hole U1387C is ~5.72 Ma (age indications at top of Fig. 3). This age is consistent with the absence of the *G. margaritae* "acme" which suggests that the bottom of the Hole must be younger than ~5.70-~5.75 Ma. The minimum timespan of the "acme" of at least 7 precession cycles makes it highly unlikely that the "acme" falls exactly in a coring gap. Within these age estimations, the two documented influxes of *G. menardii* are likely to be in the coring gap, within unrecovered Core 60R (5.550 and 5.511 Ma; stratigraphic planktic foraminifera influxes and coiling changes are represented in Fig. 8B). The dextral to sinistral coiling change of *N. acostaensis* about 809 mbsf can be closely linked to the second reported sinistral shift at 5.30 Ma in the Mediterranean, three cycles above the Miocene-Pliocene boundary (Iaccarino et al., 1999b; Lourens et al., 1996).

The depositional time span calculated on the basis of precessional cycles in Interval II and III (16 precession cycles; ~349 ky) suggests that, if the Miocene-Pliocene boundary is positioned right above Interval I, the age of the top of the studied interval is ~4.98 Ma. The precession-constrained sedimentation rates can also be used to estimate the age of the normal polarity interval from 743.99-800.65 mbsf. This suggests an age range for the normal polarity interval from ~5.04 to ~5.24 Ma. This is in good agreement with the Thvera Subchron C3n.4n which has been astronomically dated at 4.997-5.235 Ma (Lourens et al., 2004). The influx of *G. menardii* between 752.4 and 751.3 mbsf, with its age estimation from this study of about 5.07 Ma, is thus younger than the influxes recorded in NW Morocco sections (5.319 Ma; van der Laan et al., 2006; Fig. 8B). Planktic foraminifera biostratigraphy from the equivalent section in Morocco (Loulja-B) has not been studied in detail and therefore the coiling changes in *N. acostaensis* and influx of *G. menardii* may have been

overlooked so far. The well-recorded influx of *G. menardii* at 5.319 Ma in Loulja (Van der Laan et al., 2006) is most likely lost in the coring gap just after the Miocene-Pliocene boundary (Fig. 8B).

In summary, the stratigraphic interpretation which places the Miocene-Pliocene boundary at the sharp sedimentological shift at 826 mbsf, in accord with the seismic correlation (Hernández-Molina et al., 2015), and using the precession-forced, sedimentary cycles to constrain the age above and below that point, provides an age model for the studied interval of Site IODP U1387. This age model is compatible with the available foraminiferal and paleomagnetic data, which results in an age-model with three tie-points: (1) an age of about 5.7 Ma at the bottom of the hole, (2) the Miocene-Pliocene boundary (5.33 Ma) at 826 mbsf and (3) an age of about 5.0 Ma for the top of the studied interval. An uncertainty of two to three precessional cycles should be anticipated for the bottom and the top of the studied interval given the methods used to construct the age-model.

6. Discussion

Hemipelagic nannofossil muds showing significant bioturbation and containing few lithic coarser particles characterise the Messinian part (Interval I) of IODP Hole U1387C. This, combined with the relatively low Zr/Al ratios, which show no clear correlation with the precessional benthic $\delta^{18}O$ record, indicate low energy depositional environment influenced by orbital variation (Bahr et al., 2014). Similar cyclicity is found in NW Morocco and Southern Iberia, where clay-silt alternations result from orbitally-driven oscillations in detrital input (coast, riverine, or eolian; e.g. Sierro et al., 2000; van der Laan et al., 2012, Van den Berg et al., 2015). Above the Miocene-Pliocene boundary (Interval II and III), sedimentation rates are about three times higher than in Interval I and the succession has higher Zr/Al values and sand content with more abundant lithic particles (Fig. 3). This suggests significant change in the depositional environment from quiet hemipelagic conditions to a higher energy environment including the presence of weak bottom currents.

6.1 Bottom water flow strength indicators

Zr/Al ratios are relative high with large amplitude variations in Interval II and III. The sudden change in the appearance of the Zr/Al record is therefore interpreted as a shift from a low energy hemipelagic setting in Interval I, to a higher energy environment controlled by bottom currents that are subject to particle sorting in Interval II and III (Fig. 3). The suggestion of increasing energy levels is consistent with the general increase in sand content in Intervals II and III relative to the base of the Hole, especially in sections where maximum Zr/Al ratios coincide with maximum sand content (i.e. 803 to 789 mbsf; Fig. 4). Yet because of the absence of Zr/Al data from the lowermost core of Interval II (Core 57R; Fig. 3), we cannot determine with certainty from Zr/Al ratios only whether this transition occurs at the Miocene-Pliocene boundary or shortly thereafter. However, parallel behaviour between Zr/Al ratios and $\delta^{18}O$ immediately after the oldest measurement in Interval II and the abrupt sedimentation rate change reflected in benthic $\delta^{18}O$, suggests an immediate change of depositional environment over the Miocene-Pliocene boundary.

In Interval II, two sandy beds show clear bigradational grading with tracers of bioturbation (Core 54R and 55R; 788-803 mbsf; Fig. 2C, 2D, 4). The patterns represents a coarsening upward sorting from homogenous muds with sparse bioturbation to more silty/sandy deposits until the facies succession reverses. These features are characteristic of contourites (Faugères et al., 1984; Gonthier et al., 1984; Rebesco et al., 2014). Similar sedimentary sequences to the two sandy beds are characterized as contourite sequences in the Faro Drift (Gonthier et al., 1984) and recently envisioned for the Early Pleistocene for Site IODP U1386 in Alonso et al., (2016). These are distinctly different from the instantly deposited (un-bioturbated) turbiditic, normal grading, fining upwards sequences (cf. Bouma et al., 1962). Discrimination between the sand grade >63-<150 µm and >150 µm weight % confirms the hypothesis of continuous sedimentary deposition under the influence of bottom water current flow. Therefore, the two sandy beds with bi-directional grading are

interpreted as the earliest clear sandy contouritic deposits above the third precession cycle above the tentative Miocene-Pliocene boundary.

Seismic data imaging of the Early Pliocene shows features of slope instability on the Algarve Margin, north of IODP Site U1387 (Brackenridge et al., 2013; Hernández-Molina et al., 2015, 2014b; Martínez del Olmo, 2004; Roque et al., 2012). This sedimentary source may account for the tripling of the sedimentation rate that occurs at the Miocene-Pliocene boundary. However, the change in sedimentation rate is abrupt, rather than gradational, which is what would be expected if sedimentation rate changes as a result of progressive tectonic uplift of the margins and/or infilling of the basin, such as is seen in the Guadalquivir Basin (Van den Berg et al., 2015). There is also no evidence of significant shallowing of the depositional environment at Site IODP U1387 during this period. The continuous presence of benthic foraminiferal taxa which have a bathyal upper depth limit, suggest a fairly constant bathymetry throughout Intervals I to III. The increasing presence of benthic foraminiferal species limited to neritic environments from about 801 mbsf (i.e., in Interval II, ~25 m above the Miocene-Pliocene boundary) upwards are interpreted as allochthonous. They always occur alongside species with a bathyal upper depth limit and are not indicative of a significant shallowing of the water depth at Hole U1387C. The shallower benthic foraminifera are probably introduced by pulses of episodic turbiditic-like downslope transport, resulting in the cm-scale sandy layers on the upper slope (Fig. 2D; ´sand influx´ Fig. 4). In most cases, these thin turbiditic beds are almost destroyed by the combined action of bottom currents and macrobenthic communities that buried and excavate within the sediments (Dorador and Rodríguez-Tovar, 2016; Rodríguez-Tovar et al., 2015). Often only small patches of sand were preserved within a matrix of mud (Fig. 2F). If the increase in sedimentation rate was the result of instability on the Algarve margin, then this shallow-water material likely resulted from direct downslope sediment transport. If, however, the abrupt sedimentation rate increase resulted from the onset or an increase of along-slope transport, then

566 the shallow water material could derive from an up-current source. Most likely, a combination of
567 the two processes has occurred; increased slope instability due to tectonic uplift causing increased
568 sediment input from the northern Algarve Margin, while along-slope flow provided suspended load
569 from the distant Guadalquivir drainage basin, similar to the Late Pleistocene in IODP U1387 and
570 U1386 (Alonso et al., 2016). In addition, the along-slope suspended load may have been amplified
571 due to suggested tectonic uplift from the Early Pliocene (Hernández-Molina et al., 2014b). Interval
572 III shows even higher grain size fractions than Interval II, suggesting increased influence of the along-
573 and/or downslope processes. A possible increased terrigenous input from of the Guadalquivir and
574 Guadiana rivers into the Gulf of Cadiz during the warm climate of the early Pliocene (Ducassou et
575 al., 2015; Miller et al., 2005) may have amplified the along and/or downslope processes.

576 In summary, Hole U1387C shows features in Intervals II and III (lowermost Pliocene) that are
577 consistent with transport and deposition by weak along-slope bottom water currents. These
578 features are not present in Interval I (Miocene), that suggests low or absent influence of bottom
579 current flow across Site U1387. Thus, either an increase or the onset of the bottom water current
580 occurred immediately at or shortly after the Miocene-Pliocene boundary. The overall increase in
581 sand content in Intervals II and III may reflect a further increase in flow strength during the earliest
582 Pliocene. Likely, the increase in sedimentation rate at the Miocene-Pliocene boundary is the result
583 of a combination of local instability of the margins and the onset of along-slope transport.

584 ### 6.2 Origin of bottom water current flow.

585 MOW today is apparent as a warmer intermediate water mass along the margins of south west
586 Iberia penetrating the Gulf of Cadiz from the Strait of Gibraltar (Hernández-Molina et al., 2014a).
587 Consequently, if the Gibraltar Strait were closed, colder intermediate Atlantic waters would be
588 expected at the same water depths. The temperature effect should be reflected in the benthic
589 foraminiferal $\delta^{18}O$, where colder conditions and decreased MOW result in an increase in the $\delta^{18}O$

590 values. The benthic stable isotope records of NE Atlantic ODP Site 982 (1134 m water depth; Hodell
591 et al., 2001) and onshore Ain el Beida (Krijgsman et al., 2004; van der Laan et al., 2005) and Loulja
592 sections (Van der Laan et al., 2006) are compared with the benthic stable isotope record of Site
593 U1387 in order to evaluate shorter scale patterns and relative off-sets (Fig. 8). The offset of about
594 1.2 ‰ between the benthic $\delta^{18}O$ records from ODP Site 982 and NW Morocco has been interpreted
595 as the temperature difference between cold Upper North East Atlantic Deep Water (UNEADW) at
596 Site ODP 982 and warmer near-surface waters in NW Morocco in Van den Berg et al. (2015). The
597 offset between the U1387C benthic oxygen isotope record and ODP 982 is smaller than its offset
598 relative to NW Morocco, particularly during the Messinian (Fig. 8B). Ignoring the potential changes
599 in the $\delta^{18}O$ of the water, the reduced $\delta^{18}O$-offset between Site ODP 982 and IODP U1387 can
600 indicate that temperature of intermediate Atlantic waters in the Gulf of Cadiz was closer to that of
601 UNEADW in the Late Miocene. Counterintuitively, the $\delta^{18}O$ of today´s MOW is higher (0.5 to 1.1 ‰)
602 compared to NEADW (-0.1 to 0.5 ‰; Voelker et al., 2015a), however, the temperature difference
603 between these two water masses is between 8 and 10 °C. Hence the temperature effect on the shell
604 of the benthic foraminifer $\delta^{18}O$ is much higher than the effect of $\delta^{18}O$ of the water (Epstein et al.,
605 1953, 1951). This relation is evident during the transition from Marine Isotope Stage 32 to 31 in
606 IODP Hole U1387, where an increase of MOW (XRF high Zr/Al ratios) results in lower benthic
607 foraminiferal $\delta^{18}O$ (Voelker et al., 2015b). Therefore, the observed decrease in benthic $\delta^{18}O$ during
608 the early Pliocene and its stepped divergence away from ODP 982 values suggests a gradual
609 warming of intermediate Atlantic Waters near Gibraltar (Figs. 8B). The temperature increase over
610 the studied period can be attributed to the absence or minor influence of warm MOW during the
611 Messinian and the presence or increase of warmer MOW during the Pliocene. Furthermore,
612 increasing amplitudes that appear in Interval II and are even larger in Interval III may be attributed
613 to increasingly fluctuating temperatures caused by varying influences of MOW over periods of

614 insolation minima and maxima. Both arguments suggest that the increase or onset of bottom water
615 current flow over the Miocene-Pliocene boundary can be attributed to MOW. A significant
616 shallowing that would cause the change in bottom water temperatures at Site U1387C during the
617 earliest Pliocene is excluded based on the benthic foraminifera analyses.
618 Interestingly, amplitudes of benthic $\delta^{18}O$ at Site U1387 do not only increase over the Miocene-
619 Pliocene boundary, but also during the Messinian they are larger than amplitudes at Site ODP 982,
620 Ain el Beida and Loulja. The Montemayor core reveals the same feature as U1387C (Pérez-Asensio
621 et al., 2012; Van den Berg et al., 2015). The difference in amplitude of Hole U1387 and ODP 982
622 must be attributed to either a relative change of $\delta^{18}O$ in the water mass or temperature. Increased
623 amplitudes during the Pliocene can be attributed to fluctuations in MOW, however, it is thought
624 that during the Messinian Salinity Crisis MOW was either extensively reduced or even absent
625 (Flecker et al., 2015). Larger amplitudes due to larger temperature changes of shallower water
626 depths can be excluded, because the shallower Loulja and Ain el Beida do not show the larger
627 amplitudes. These sites are closer to the thermocline and thus more sensitive to temperature
628 changes on glacial-interglacial cycles. One alternative, however speculative since there are no flow
629 strength indicators observed in the sediments, is that the relatively high amplitude variations in
630 benthic $\delta^{18}O$ in U1387C compared with both shallower and deeper locations hint towards the
631 presence of weak MOW during the Messinian.
632

Conclusions

We present evidence that the flow of Mediterranean-Atlantic bottom water began very shortly after the Messinian Salinity Crisis in the Gulf of Cadiz from IODP Site U1387. This study provides a chronostratigraphic framework for the lower part of IODP Site U1387C utilising biostratigraphic, paleomagnetic, and cyclostratigraphic constraints. Our data suggest that the record extends into the latest Messinian and includes the Miocene-Pliocene boundary. Seismic data linking Site U1387C and the Algarve-2 well, as well as sedimentary changes in the sequence itself constrains the Miocene-Pliocene boundary to around 826 mbsf. Sediment deposition during the latest Messinian in the Gulf of Cadiz took place in a relatively quiet, hemipelagic environment driven by precessionally controlled Mediterranean monsoonal induced oscillations, with negligible evidence of bottom water flow strength. During the earliest Pliocene, an immediate decrease in the benthic $\delta^{18}O$ may be the result from the direct warming of Atlantic Intermediate waters due to increased Mediterranean-Atlantic exchange. The increase in sedimentation rate and as well as elevated variable Zr/Al ratios could have resulted from the onset of weak along-slope bottom water currents immediately at or right after the Miocene-Pliocene boundary. The occurrence of contouritic sedimentation in the Gulf of Cadiz results in tow bigradational sandy beds above the third precession cycles after the Miocene-Pliocene boundary. Shallow water benthic foraminifers indicate that, besides along-slope transport, down-slope transport was present, redistributing shallow marine (continental shelf) particles to the upper slope.

653 Acknowledgements: We acknowledge the MEDGATE-team for passionate discussions and valuable
654 comments on this study. David Hodell is thanked for the stable isotope analyses in the Godwin
655 Laboratory for Palaeoclimate Research at the University of Cambridge and his valuable comments
656 on the manuscript. This research used samples and data collected through the Integrated Ocean
657 Drilling Program. Rocío Marino Ferrero and Jose Ignacio Martín Cruz are acknowledged for washing
658 sediment samples. The research leading to these results has received funding from the People
659 Programme (Marie Curie Actions) of the European Union's Seventh Framework Programme
660 FP7/2007-2013/ under REA Grant Agreement No. 290201 MEDGATE, project P25831-N29 of the
661 Austrian Science Fund (FWF), and NSF Grant OCE-1426132. The research was partially supported
662 through Castilla y Leon project SA263U14 and CTM 2012-39599-C03, IGCP-619, and INQUA 1204
663 Projects. Research was conducted in the framework of the Continental Margins Research Group of
664 the Royal Holloway University of London. We also thank A. Bahr and A. Voelker for full and
665 constructive reviews that improved the manuscript.

666

References

Alonso, B., Ercilla, G., Casas, D., Stow, D.A.V., Rodríguez-Tovar, F.J., Dorador, J., Hernández-Molina, F.-J., 2016. Contourite vs gravity-flow deposits of the Pleistocene Faro Drift (Gulf of Cadiz): Sedimentological and mineralogical approaches. Marine Geology (in press). doi:10.1016/j.margeo.2015.12.016

Bahr, A., Jiménez-Espejo, F.J., Kolasinac, N., Grunert, P., Hernández-Molina, F.J., Rohl, U., Voelker, A.H.L., Escutia, C., Stow, D.A. V., Hodell, D.A., Alvarez-Zarikian, C.A., 2014. Deciphering bottom current velocity and paleoclimate signals from contourite deposits in the Gulf of Cádiz during the last 140 kyr: an inorganic geochemical approach. Geochemistry Geophysics Geosystems 18, 1–16. doi:10.1002/2014GC005356

Bahr, A., Kaboth, S., Jiménez-Espejo, F.J., Sierro, F.J., Voelker, A.H.L., Lourens, L., Röhl, U., Reichart, G.J., Escutia, C., Hernández-Molina, F.J., Pross, J., Friedrich, O., 2015. Persistent monsoonal forcing of Mediterranean Outflow Water dynamics during the late Pleistocene. Geology 43, 951–954. doi:10.1130/G37013.1

Benson, H., Rakic-El Bied, K., Bonaduce, G., 1991. An important current reversal (influx) in the Rifian corridor (Morocco) at the Tortonian-Messinian boundary: The end of Tethys ocean. Paleoceanography 6, 164–192.

Berger, A., 1984. Accuracy and frequency stability of the Earth´s orbital elements during the Quaternary, in: A. Berger, Imbrie, J., Hays, H., Kukla, G., Saltzman, B. (Eds.), Milankovitch and Climate: Understanding the Response to Astronomical Forcing. D. Reidel Publishing, Dordrecht, p. 3.

Bertrand, S., Hughen, K.A., Sepúlveda, J., Pantoja, S., 2012. Geochemistry of surface sediments from the fjords of Northern Chilean Patagonia (44-47°S): Spatial variability and implications for paleoclimate reconstructions. Geochimica et Cosmochimica Acta 76, 125–146. doi:10.1016/j.gca.2011.10.028

Blanc, P.-L., 2002. The opening of the Plio-Quaternary Gibraltar Strait: assessing the size of a cataclysm. Geodinamica Acta 15, 303–317.

Bouma, A.H., Kuenen, P.H., Shepard, F.P., 1962. Sedimentology of some flysch deposits: a graphic approach to facies interpretation. Elsevier, Amsterdam.

Brackenridge, R.E., Hernández-Molina, F.J., Stow, D. a. V., Llave, E., 2013. A Pliocene mixed contourite–turbidite system offshore the Algarve Margin, Gulf of Cadiz: Seismic response, margin evolution and reservoir implications. Marine and Petroleum Geology 46, 36–50. doi:10.1016/j.marpetgeo.2013.05.015

Dorador, J., Rodríguez-Tovar, F.J., 2016. High resolution digital image treatment to color analysis on cores from IODP expedition 339: Approaching lithologic features and bioturbational influence. Marine Geology (in press). doi:10.1016/j.margeo.2016.02.005

Ducassou, E., Fournier, L., Sierro, F.J., Zarikian, C.A.A., Lo, J., Flores, J.A., Roque, C., 2015. Origin of the large Pliocene and Pleistocene debris fl ows on the Algarve margin (in press). doi:10.1016/j.margeo.2015.08.018

Duggen, S., Hoernle, K., Bogaard, P. van den, Rüpke, L., Morgan, J.P., 2003. Deep roots of the Messinian salinity crisis. Nature 422, 602–606. doi:10.1038/nature01551.1.

Epstein, S., Buchsbaum, R., Lowenstam, H. a, Urey, H.C., 1953. Revised Carbonate-Water Isotopic Temeprature Scale. Geological Society of America Bulletin 64, 1315–1325. doi:10.1130/0016-7606(1953)64

Epstein, S., Buchsbaum, R., Lowenstam, H.A., Urey, H.C., 1951. Carbonate-water isotopic temperature scale. Bulletin of the Geological Society of America 62, 417–426. doi:10.1017/CBO9781107415324.004

714 Expedition 339 Scientists, 2013a. Site U1387, in: Stow, D.A.V., Hernández-Molina, F.J., Alvarez-
715 Zarikian, C.A., Expedition 339 Scientists (Eds.), Proceedings of the Intergrated Ocean Drilling
716 Program. Integrated Ocean Drilling Program Management International, Inc, Tokyo.
717 doi:10.2204/iodp.proc.339.105.2013
718 Expedition 339 Scientists, 2013b. Methods, in: Stow, D.A.V., Hernández-Molina, F.J., Alvarez
719 Zarikian, C.A., Expedition 339 Scientists (Eds.), Proceedings of the IODP 339. Integrated
720 Ocean Drilling Program Management International, Inc, Tokyo, pp. 1–5.
721 doi:doi:10.2204/iodp.proc.339.102.2013
722 Expedition 339 Scientists, 2012. Mediterranean outflow: environmental significance of the
723 Mediterranean Outflow Water and its global implications. IODP preliminary Report 339.
724 doi:10.2204/iodp.pr.339.2012
725 Faugères, J., Gonthier, E., Stow, D.A.V., 1984. Contourite drift molded by deep Mediterranean
726 outflow. Geology 12, 296–300.
727 Flecker, R., Krijgsman, W., Capella, W., de Castro Martíns, C., Dmitrieva, E., Mayser, J.P.,
728 Marzocchi, A., Modestu, S., Lozano, D.O., Simon, D., Tulbure, M., van den Berg, B., van der
729 Schee, M., de Lange, G., Ellam, R., Govers, R., Gutjahr, M., Hilgen, F., Kouwenhoven, T., Lofi,
730 J., Meijer, P., Sierro, F.J., Bachiri, N., Barhoun, N., Alami, A.C., Chacon, B., Flores, J. a.,
731 Gregory, J., Howard, J., Lunt, D., Ochoa, M., Pancost, R., Vincent, S., Yousfi, M.Z., 2015.
732 Evolution of the Late Miocene Mediterranean-Atlantic gateways and their impact on regional
733 and global environmental change. Earth-Science Reviews 150, 365–392.
734 doi:10.1016/j.earscirev.2015.08.007
735 Flores, J.A., Sierro, F.J., 1997. A revised technique for the estimation of nannofossil accumulation
736 rates. Micropaleontology 43, 321–324.
737 Flores, J.A., Sierro, F.J., Filippelli, G.M., Bárcena, M.Á., Pérez-Folgado, M., Vázquez, A., Utrilla, R.,
738 2005. Surface water dynamics and phytoplankton communities during deposition of cyclic
739 late Messinian sapropel sequences in the western Mediterranean. Marine Micropaleontology
740 56, 50–79. doi:10.1016/j.marmicro.2005.04.002
741 Ganeshram, R.S., Calvert, S.E., Pedersen, T.F., Cowie, G.L., 1999. Factors controlling the burial of
742 organic carbon in laminated and bioturbated sediments off NW Mexico: Implications for
743 hydrocarbon preservation. Geochimica et Cosmochimica Acta 63, 1723–1734.
744 doi:10.1016/S0016-7037(99)00073-3
745 Gonthier, E., Faugères, J., Stow, D.A.V., 1984. Contourite facies of the Faro drift, Gulf of Cadiz.
746 Geological Society, London, Special Publications1 15, 275–292.
747 Hernández-Molina, F.J., Llave, E., Preu, B., Ercilla, G., Fontan, A., Bruno, M., Serra, N., Gomiz, J.J.,
748 Brackenridge, R.E., Sierro, F.J., Stow, D. a. V., Garcia, M., Juan, C., Sandoval, N., Arnaiz, A.,
749 2014a. Contourite processes associated with the Mediterranean Outflow Water after its exit
750 from the Strait of Gibraltar: Global and conceptual implications. Geology 42, 227–230.
751 doi:10.1130/G35083.1
752 Hernández-Molina, F.J., Sierro, F.J., Llave, E., Roque, C., Stow, D.A.V., Williams, T., Lofi, J., Van der
753 Schee, M., Arnaíz, A., Ledesma, S., Rosales, C., Rodríguez-Tovar, F.J., Pardo-Igúzquiza, E.,
754 Brackenridge, R.E., 2015. Evolution of the gulf of Cadiz margin and southwest Portugal
755 contourite depositional system: Tectonic, sedimentary and paleoceanographic implications
756 from IODP expedition 339. Marine Geology (in press). doi:10.1016/j.margeo.2015.09.013
757 Hernández-Molina, F.J., Stow, D. a. V., Alvarez-Zarikian, C. a., Acton, G., Bahr, A., Balestra, B.,
758 Ducassou, E., Flood, R., Flores, J. -a., Furota, S., Grunert, P., Hodell, D., Jimenez-Espejo, F.,
759 Kim, J.K., Krissek, L., Kuroda, J., Li, B., Llave, E., Lofi, J., Lourens, L., Miller, M., Nanayama, F.,
760 Nishida, N., Richter, C., Roque, C., Pereira, H., Sanchez Goñi, M.F., Sierro, F.J., Singh, a. D.,
761 Sloss, C., Takashimizu, Y., Tzanova, A., Voelker, A., Williams, T., Xuan, C., 2014b. Onset of

762 Mediterranean outflow into the North Atlantic. Science 344, 1244–1250.
763 doi:10.1126/science.1251306
764 Hernández-Molina, J., Llave, E., Somoza, L., Fernández-Puga, M.C., Maestro, A., León, R.,
765 Medialdea, T., Barnolas, A., García, M., Díaz del Río, V., Fernández-Salas, L.M., Vázquez, J.T.,
766 Lobo, F., Alveirinho Dias, J.M., Rodero, J., Gardner, J., 2003a. Looking for clues to
767 paleoceanographic imprints: A diagnosis of the Gulf of Cadiz contourite depositional systems.
768 Geology 31, 19–22.
769 Hernández-Molina, J., Llave, E., Somoza, L., Fernández-puga, M.C., Maestro, A., León, R.,
770 Medialdea, T., Barnolas, A., García, M., Díaz, V., Miguel, L., Vázquez, J.T., Lobo, F., Dias,
771 J.M.A., Rodero, J., Gardner, J., Herna, J., Ciencias, F. De, Vigo, U. De, Ferna, M.C., Leo, R.,
772 Ferna, L.M., 2003b. Looking for clues to paleoceanographic imprints : A diagnosis of the Gulf
773 of Cadiz contourite depositional systems. Geology 31, 19–22. doi:10.1130/0091-
774 7613(2003)031<0019
775 Hilgen, F.., Lourens, L.., Van Dam, J.A., 2012. The Neogene Period, in: Gradstein, F.M., Ogg, J.G.,
776 Schmitz, M., Ogg, G. (Eds.), The Geologic Time Scale. Elsevier, Amsterdam, pp. 923–978.
777 doi:doi:10.1016/B978-0-444-59425-9.01001-5
778 Hilgen, F.J., Krijgsman, W., 1999. Cyclostratigraphy and astrochronology of the Tripoli diatomite
779 formation (pre-evaporite Messinian, Sicily, Italy). Terra Nova 11, 16–22.
780 Hodell, D.A., Benson, R.H., Kent, D. V, Boersma, A., Rakic-El Bied, K., 1994. Magnetostratigraphic,
781 biostratigraphic, and stable isotope stratigraphy of an Upper Miocene drill core from the Salé
782 Briqueterie (northern Morocco): A high-resolution chronology for the Messinian stage.
783 Paleoceanography 9, 835–855.
784 Hodell, D.A., Curtis, J.H., Sierro, J., Raymo, M.E., 2001. Correlation of Late Miocene to Early
785 Pliocene sequences between the Mediterranean and North Atlantic. Paleoceanography 16,
786 164–178.
787 Hsu, K.J., Ryan, W.B.., Cita, M.B., 1973. Late Miocene desiccation of the Mediterranean. Nature
788 242, 240–244.
789 Iaccarino, S., Castradori, D., Cita, M., 1999. The Miocene/Pliocene boundary and the significance of
790 the earliest Pliocene flooding in the Mediterranean. Memorie Società Geologica Italiana 54,
791 109–131.
792 Iaccarino, S.M., Cita, M.B., Gaboardi, S., Gruppini, G.M., 1999. High-resolution biostratigraphy at
793 the Miocene/Pliocene boundary in Holes 974B and 975B, western Mediterranean.
794 Proceedings of the Intergrated Ocean Drilling Program, Scientific Results 161, 197–221.
795 Ivanovic, R.F., Valdes, P.J., Flecker, R., Gutjahr, M., 2014. Modelling global-scale climate impacts of
796 the late Miocene Messinian Salinity Crisis. Climate of the Past 10, 607–622. doi:10.5194/cp-
797 10-607-2014
798 Jones, R.W., 1994. The Challenger foraminifera. Oxford University Press, Oxford, New York.
799 Kaboth, S., Bahr, A., Reichart, G.-J., Jacobs, B., Lourens, L.J., 2015. New insights into upper MOW
800 variability over the last 150kyr from IODP 339 Site U1386 in the Gulf of Cadiz. Marine
801 Geology (in press). doi:10.1016/j.margeo.2015.08.014
802 Kirschvink, J.L., 1980. The least-squares line and plane and the analysis of paleomagnetic data.
803 Geophysical Journal of the Royal Astronomical Society 62, 699–718. doi:10.1111/j.1365-
804 246X.1980.tb02601.x
805 Krijgsman, W., Gaboardi, S., Hilgen, F.J., Iaccarino, S., De Kaenel, E., van der Laan, E., 2004. Revised
806 astrochronology for the Ain el Beida section (Atlantic Morocco): No glacio-eustatic control for
807 the onset of the Messinian Salinity Crisis. Stratigraphy 1, 87–101.
808 Krijgsman, W., Langereis, C.., Zachariasse, W.., Boccaletti, M., Moratti, G., Gelati, R., Iaccarino, S.,
809 Papani, G., Villa, G., 1999. Late Neogene evolution of the Taza–Guercif Basin (Rifian Corridor,

Morocco) and implications for the Messinian salinity crisis. Marine Geology 153, 147–160. doi:10.1016/S0025-3227(98)00084-X
Kuroda, J., Jiménez-Espejo, F.J., Nozaki, T., Gennari, R., Lugli, S., Manzi, V., Roveri, M., Flecker, R., Sierro, F.J., Yoshimura, T., Suzuki, K., Ohkouchi, N., 2016. Miocene to Pleistocene osmium isotopic records of the Mediterranean sediments. Paleoceanography 31, 148–166. doi:10.1002/2015PA002853
Lamy, F., Arz, H.W., Kilian, R., Lange, C.B., Lembke-Jene, L., Wengler, M., Kaiser, J., Baeza-Urrea, O., Hall, I.R., Harada, N., Tiedemann, R., 2015. Glacial reduction and millennial-scale variations in Drake Passage throughflow. Proceedings of the National Academy of Sciences of the United States of America 112, 13496–501. doi:10.1073/pnas.1509203112
Laskar, J., Robutel, P., Joutel, F., Gastineau, M., Correia, A.C.M., Levrard, B., 2004. A long-term numerical solution for the insolation. Astronomy & Astrophysics 285, 261–285.
Leckie, R.M., Olson, H.C., 2003. Foraminifera as proxies for sea-level change on siliciclastic margins. In: Micropaleontologic Proxies for Sea-Level Change and Stratigraphic Discontinuities. SEPM Special Publication 75, 5–19.
Ledesma, S., 2000. Astrobiocronología y estratigrafía de alta resolución del neógeno de la cuenca del Guadalquivir-Golfo de Cádiz.
Lisiecki, L.E., Raymo, M.E., 2005. A Pliocene-Pleistocene stack of 57 globally distributed benthic δ 18 O records. Paleoceanography 20, PA1003. doi:10.1029/2004PA001071
Lofi, J., Gorini, C., Berné, S., Clauzon, G., Tadeu Dos Reis, a., Ryan, W.B.F., Steckler, M.S., 2005. Erosional processes and paleo-environmental changes in the Western Gulf of Lions (SW France) during the Messinian Salinity Crisis. Marine Geology 217, 1–30. doi:10.1016/j.margeo.2005.02.014
Lofi, J., Voelker, A.H.L., Ducassou, E., Hernández-Molina, F.J., Sierro, F.J., Bahr, A., Galvani, A., Lourens, L.J., Pardo-Igúzquiza, E., Pezard, P., Rodríguez-Tovar, F.J., Williams, T., 2015. Quaternary chronostratigraphic framework and sedimentary processes for the Gulf of Cadiz and Portuguese Contourite Depositional Systems derived from Natural Gamma Ray records. Marine Geology (in press). doi:10.1016/j.margeo.2015.12.005
Lourens, L.J., Antonarakou, A., Hilgen, F.J., Hoof, A.A.M. Van, Zachariasse, W.J., 1996. Evaluation of the Plio-Pleistocene astronomical timescale. Paleoceanography 11, 391–413.
Lourens, L.J., Hilgen, F., Shackleton, J., Laskar, J., Wilson, J., 2004. The Neogene period, in: Gradstein, F., Ogg, J., Simth, A. (Eds.), A Geologic Time Scale. Cambridge University Press, London, pp. 409–440.
Martínez del Olmo, W., 2004. La exploración de hidrocarburos en el Terciario de España. Boletín Geológico y Minero 115, 411–426.
McLennan, S.M., Hemming, S., McDaniel, D.K., Hanson, G.N., 1993. Geochemical approaches to sedimentation, provenance, and tectonics. Geological Society of America Special Paper 284, 21–40. doi:10.1130/SPE284-p21
Meijer, P.T., Krijgsman, W., 2005. A quantitative analysis of the desiccation and re-filling of the Mediterranean during the Messinian Salinity Crisis. Earth and Planetary Science Letters 240, 510–520. doi:10.1016/j.epsl.2005.09.029
Mendes, I., Alveirinho Dias, J.M., Schonfeld, J., Ferreira, J., 2012. Distribution of living benthic foraminifera on the northern Gulf of Cadiz continental shelf. The Journal of Foraminiferal research 42, 18–38. doi:10.2113/gsjfr42.1.18
Miller, K.G., Kominz, M.A., Browning, J. V, Wright, J.D., Mountain, G.S., Katz, M.E., Sugarman, P.J., Cramer, B.S., Pekar, S.F., Science, S., Series, N., Nov, N., 2005. The Phanerozoic Record of Global Sea-Level Change 310, 1293–1298.
Ohneiser, C., Florindo, F., Stocchi, P., Roberts, A.P., DeConto, R.M., Pollard, D., 2015. Antarctic

glacio-eustatic contributions to late Miocene Mediterranean desiccation and reflooding. Nature Communications 6, 8765. doi:10.1038/ncomms9765

Pérez-Asensio, J.N., Aguirre, J., Jiménez-Moreno, G., Schmiedl, G., Civis, J., 2013. Glacioeustatic control on the origin and cessation of the Messinian salinity crisis. Global and Planetary Change 111, 1–8. doi:10.1016/j.gloplacha.2013.08.008

Pérez-Asensio, J.N., Aguirre, J., Schmiedl, G., Civis, J., 2014. Messinian productivity changes in the northeastern Atlantic and their relationship to the closure of the Atlantic-Mediterranean gateway: implications for Neogene palaeoclimate and palaeoceanography. Journal of the Geological Society 171, 389–400. doi:10.1144/jgs2013-032

Pérez-Asensio, J.N., Aguirre, J., Schmiedl, G., Civis, J., 2012. Impact of restriction of the Atlantic-Mediterranean gateway on the Mediterranean Outflow Water and eastern Atlantic circulation during the Messinian. Paleoceanography 27, PA3222. doi:10.1029/2012PA002309

Phipps, M., Jorissen, F.., Pusceddu, A., Bianchelli, S., de Stichter, H., 2012. Live benthic foraminiferal fauna along a bathymetrical transect (282-4987 m) on the Portuguese margin (NE Atlantic). Journal of Foraminiferal Research 42, 66–81. doi:doi: 10.2113/gsjfr.42.1.66

Raffi, I., Backman, J., Fornaciari, E., Pälike, H., Rio, D., Lourens, L., Hilgen, F., 2006. A review of calcareous nannofossil astrobiochronology encompassing the past 25 million years. Quaternary Science Reviews 25, 3113–3137. doi:10.1016/j.quascirev.2006.07.007

Rebesco, M., Javier Hernández-Molina, F., Van Rooij, D., Wåhlin, A., 2014. Contourites and associated sediments controlled by deep-water circulation processes: State-of-the-art and future Considerations. Marine Geology 352, 111–154. doi:10.1016/j.margeo.2014.03.011

Rodríguez-Tovar, F.J., Dorador, J., Martin-Garcia, G.M., Sierro, F.J., Flores, J.A., Hodell, D.A., 2015. Response of macrobenthic and foraminifer communities to changes in deep-sea environmental conditions from Marine Isotope Stage (MIS) 12 to 11 at the “Shackleton Site.” Global and Planetary Change 133, 176–187. doi:10.1016/j.gloplacha.2015.08.012

Rogerson, M., Bigg, G.R., Rohling, E.J., Ramírez, J., 2012a. Vertical density gradient in the eastern North Atlantic during the last 30,000 years. Climate Dynamics 39, 589–598. doi:10.1007/s00382-011-1148-4

Rogerson, M., Rohling, E.J., Bigg, G.R., Ramirez, J., 2012b. Paleoceanography of the Atlantic-Mediterranean exchange: Overview and first quantitative assessment of climatic forcing. REVIEWS OF GEOPHYSICS 50.

Rogerson, M., Rohling, E.J., Weaver, P.P.E., Murray, J.W., 2005. Glacial to interglacial changes in the settling depth of the Mediterranean Outflow plume. Paleoceanography 20, 1–12. doi:10.1029/2004PA001106

Roque, C., Duarte, H., Terrinha, P., Valadares, V., Noiva, J., Cachao, M., Ferreira, J., Legoinha, P., Zitellini, N., 2012. Pliocene and Quarternary depositional model of the Algarve margin contourite drifts (Gulf of Cadiz, SW Iberia): Seismic architecture, tectonic control and paleoceanographic insights. Marine Geology 303-306, 42–62.

Roveri, M., Flecker, R., Krijgsman, W., Lofi, J., Lugli, S., Manzi, V., Sierro, F.J., Bertini, A., Camerlenghi, A., De Lange, G., Govers, R., Hilgen, F.J., Hübscher, C., Meijer, P.T., Stoica, M., 2014. The Messinian Salinity Crisis: Past and future of a great challenge for marine sciences. Marine Geology 352, 25–58. doi:10.1016/j.margeo.2014.02.002

Santisteban, C., Taberner, C., 1983. Shallow marine and continental conglomerates derived from coral reef complexes after desiccation of a deep marine basin : the Tortonian-Messinian deposits of the Fortuna Basin , SE Spain. Journal of the Geological Society of London 140, 401–411.

Schönfeld, J., 2002. Recent benthic foraminiferal assemblages in deep high-energy environments from the Gulf of Cadiz (Spain). Micropaleontology 44, 141–162.

906 Schönfeld, J., 1997. The impact of the Mediterranean Outflow Water (MOW) on benthic
907 foraminiferal assemblages and surface sediments at the southern Portuguese continental
908 margin. Marine Micropaleontology 29, 211–236. doi:10.1016/S0377-8398(96)00050-3
909 Shackleton, N.J., Hall, M.A., Pate, D., 1995. Pliocene stable isotope stratigraphy of Site 846.
910 Proceedings of the Intergrated Ocean Drilling Program 138, 337–355.
911 Sierro, F.J., Civis, J., González Delgado, J. a, 1982. Estudio de los Foraminíferos del Neogeno de
912 Niebla (Huelva). Studia Geologica Salmanticensia 17, 67–87.
913 Sierro, F.J., Flores, J.A., Civis, J., González Delgado, J.A., Francés, G., 1993. Late Miocene
914 globorotaliid event-stratigraphy and biogeography in the NE-Atlantic and Mediterranean.
915 Marine Micropaleontology 21, 143–168.
916 Sierro, F.J., Hilgen, F.J., Krijgsman, W., Flores, J.A., 2001. The Abad composite (SE Spain): a
917 Messinian reference section for the Mediterranean and the APTS. Palaeogeography,
918 Palaeoclimatology, Palaeoecology 168, 141–169.
919 Sierro, F.J., Ledesma, S., Flores, J., Torrescusa, S., Olmo, M., 2000. Sonic and gamma-ray
920 astrochronology : Cycle to cycle calibration of Atlantic climatic records to Mediterranean
921 sapropels and astronomical oscillations. Geology 28, 695–698. doi:10.1130/0091-
922 7613(2000)28<695
923 Simon, D., Meijer, P., 2015. Dimensions of the Atlantic-Mediterranean connection that caused the
924 Messinian Salinity Crisis. Marine Geology. doi:10.1016/j.margeo.2015.02.004
925 Stow, D.A.V., Hernández-Molina, F.J., Alvarez Zarikian, C.A., Scientists, the E. 339, 2013.
926 Proceedings IODP 339, Intergrated Ocean Drilling Program Management International.
927 Tokyo. doi:doi:10.2204/iodp.proc.339.2013
928 Stow, D.A.V., Hernández-Molina, F.J., Hodell, D., Alvarez Zarikian, C.A., 2011. Mediterranean
929 Outflow: environmental significance of the Mediterranean Outflow Water and its global
930 implications. IODP Scientific Prospectus 339. doi:10.2204/iodp.sp.339.2011
931 Van Couvering, J., Castradori, D., Cita, M.B., Hilgen, F.J., Domenico, R., 2000. The base of the
932 Zanclean Stage and of the Pliocene Series. Episodes 23, 179–187.
933 Van den Berg, B.C.J., Sierro, F.J., Hilgen, F.J., Flecker, R., Larrasoaña, J.C., Krijgsman, W., Flores, J.
934 a., Mata, M.P., Bellido Martín, E., Civis, J., González-Delgado, J. a., 2015. Astronomical tuning
935 for the upper Messinian Spanish Atlantic margin: Disentangling basin evolution, climate
936 cyclicity and MOW. Global and Planetary Change 135, 89–103.
937 doi:10.1016/j.gloplacha.2015.10.009
938 Van der Laan, E., Gaboardi, S., Hilgen, F.J., Lourens, L.J., 2005. Regional climate and glacial control
939 on high-resolution oxygen isotope records from Ain el Beida (latest Miocene, northwest
940 Morocco): A cyclostratigraphic analysis in the depth and time domain. Paleoceanography 20,
941 PA1001. doi:10.1029/2003PA000995
942 Van der Laan, E., Hilgen, F.J., Lourens, L.J., de Kaenel, E., Gaboardi, S., Iaccarino, S., 2012.
943 Astronomical forcing of Northwest African climate and glacial history during the late
944 Messinian (6.5–5.5Ma). Palaeogeography, Palaeoclimatology, Palaeoecology 313-314, 107–
945 126. doi:10.1016/j.palaeo.2011.10.013
946 Van der Laan, E., Snel, E., de Kaenel, E., Hilgen, F.J., Krijgsman, W., 2006. No major deglaciation
947 across the Miocene-Pliocene boundary: Integrated stratigraphy and astronomical tuning of
948 the Loulja sections (Bou Regreg area, NW Morocco). Paleoceanography 21, 1–27.
949 doi:10.1029/2005PA001193
950 Van Morkhoven, F.P., Berggren, W.A., Edwards, A.S., Oertli, H.J., 1986. Cenozoic cosmopolitan
951 deep-water benthic foraminifera. Bulletin des Centres de Recherches Exploration-Production
952 Elf-Aquitaine: Memorie 11, 68–70.
953 Voelker, A., Lebreiro, S., Schonfeld, J., Cacho, I., Erlenkeuser, H., Abrantes, F., 2006. Mediterranean

954 outflow strengthening during northern hemisphere coolings: A salt source for the glacial
955 Atlantic? Earth and Planetary Science Letters 245, 39–55. doi:10.1016/j.epsl.2006.03.014
956 Voelker, A.H.L., Colman, A., Olack, G., Waniek, J.J., Hodell, D., 2015a. Oxygen and hydrogen isotope
957 signatures of Northeast Atlantic water masses. Deep Sea Research Part II: Topical Studies in
958 Oceanography 116, 89–106. doi:10.1016/j.dsr2.2014.11.006
959 Voelker, A.H.L., Salgueiro, E., Rodrigues, T., Jimenez-Espejo, F.J., Bahr, A., Alberto, A., Loureiro, I.,
960 Padilha, M., Rebotim, A., Röhl, U., 2015b. Mediterranean Outflow and surface water
961 variability off southern Portugal during the early Pleistocene: A snapshot at Marine Isotope
962 Stages 29 to 34 (1020–1135ka). Global and Planetary Change 133, 223–237.
963 doi:10.1016/j.gloplacha.2015.08.015
964 Young, J.R., Flores, J.A., Wei, W., 1994. A summary chart of Neogene Nannofossil
965 magnetobiostratigraphy. Journal of nannoplankton research 16, 21–27.

966

Tables captions

Table 1. Planktic biostratigraphic events used in the present study and their position (mbsf) in IODP Hole U1387C and if it is stated in the preliminary IODP report (Expedition 339 Scientist, 2012). FO = First Occurrence, LO = Last Occurrence.

Table 2. Wavelengths of cyclical alternations of $\delta^{18}O$ for selected intervals. *Three cyclical alternations are visible in the $\delta^{18}O$ record plus an additional cycle visible in $\delta^{13}C$ is taken into consideration.

Figure captions

Figure 1. Hydrography of the Gulf of Cadiz showing the main modern flow paths of MOW, specified as the Upper and Lower branch (modified after Hernández-Molina et al., 2003). Locations of IODP Site U1386 and U1387, Algarve-2, Site ODP 982, MD01-2444, the onshore Montemayor-1 core in SW Spain and exposed section of Ain el Beida/Loulja in NW Morocco are indicated.

Figure 2. Representative photographs of core sections from each interval (A-E). Coloured Xs indicate their positions in the hole, along with the iODP sample name that gives the precise location of the image (A) Sharp contact within greenish grey to very dark greenish grey nannofossil mud with colour alternation in a sandy interval. Bioturbation is visible (746.25 to 746.55 mbsf). (B) Cemented sandstone with biogenic carbonate (749.48 to 749.63 mbsf.). (C) Homogenous sandier sediments (Interval II, 790.28 to 790.43 mbsf). (D) Thin 2 cm beds of dark greenish grey silty sand (792.61 to 792.76 mbsf). (E) Distinct bioturbation with smaller average grain size (842.25 to 842.40 mbsf). (F) Small patches of sand preserved within a matrix of mud excavated by macrobenthic communities (771.62 to 771.86 mbsf). (G) 5-point moving average (black) of the colour reflectance (L*) (open grey circles) is compared with darker colours of the core pictures with brown shades.

Figure 3. Palaeo climate records of IODP Site U1387C from 730-865 mbsf. Intervals I, II and III, magnetostratigraphic polarities, core numbers and their recovery, and colour changes from core photographs are shown above the charts (Expedition 339 Scientists, 2013a). Green shaded areas indicate darker colours in core photographs. Age ranges are displayed on top of the graph. (A) $\delta^{18}O$ of benthic *Cibicidoides pachyderma* >250 µm. Grey horizontal bars show average $\delta^{18}O$ values per interval. (B) Elemental Zr/Al ratios with five point moving average in black. (C) Weight % sand >63 µm as a percentage of total dry weight.

Figure 4. Grain size fractions from >63 to <150 µm (orange) and >150 µm (red) from 788 to 806 mbsf. Core numbers and pictures are displayed on top of the graph. Two outliers are explained by presence of pyrite and a centimetre scale sand influx (visible on core photos). The distinct increase and decrease in the grain size fraction are indicating the bigradational pattern (accentuated with black arrows).

Figure 5. Planktic foraminifera biostratigraphy of Site U1387. Relative abundances are displayed. The light blue shaded area shows the "acme" of *G. margaritae*. The %dex *N. acostaensis* displays the relative distribution of dex/(dex+sin) of *N. acostaensis.* The purple shaded area indicates that most species have dextral coiling. The two arrows highlight dextral to sinistral coiling changes.

Figure 6. Magnetostratigraphic interpretation for magnetozones between 550 mbsf and the base of Hole U1387C. The inclinations plotted are the preferred inclinations determined by principal component analysis (PCA), and are given in the Supplementary Data. The symbols reflect the different quality of the results as discussed in the text and Supplementary Data Quality 3 (red circles), Quality 4 (blue squares), and Quality 5 (green triangles), which are plotted along the 0° inclination merely to show the depth at which they occur.

Figure 7. Chronostratigraphy for Site U1387 from magnetostratigraphic and biostratigraphic constraints.

Figure 8. (A) Normalized precession-Tilt (obliquity; P-T) and tilt of the La04 solution (65°N summer insolation; Laskar et al., 2004), red highlights the clear resemblance with the Loulja $\delta^{18}O$ record. (B) Benthic $\delta^{18}O$ record of *Cibicidoides pachyderma* of core U1387C (dotted blue) for the constructed tentative age-model with its three tie-points at 5.0, 5.33 and 5.72 Ma. Horizontal boxes show the average of IODP U1387 for the different Intervals. $\delta^{18}O$ of *Planulina ariminensis* of Ain el Beida (Krijgsman et al., 2004; Van der Laan et al., 2005), Loulja (Van der Laan et al., 2006) and ODP982 (corrected according to Van der Laan et al., 2006; Hodell et al., 2001) and the LR04-stack (Lisiecki and Raymo, 2005) are displayed as references. Influxes of *Globorotalia menardii* (*G. men*) of Loulja, Ain el Beida and U1387C are indicated with arrows as well as the dextral to sinistral coiling change of *Neogloboquadrina acostaensis* (sin *N. aco*) in U1387C. TG stages are taken from Site ODP 846 (Shackleton et al., 1995), while T stages are used from the LR04- stack. Typically, there is a strong 1:1 correlation between *P. ariminensis* and *C. pachyderma*, especially for $\delta^{18}O$ (e.g. van der Laan et al., 2006; Voelker et al., 2015). (C) Insolation curve with solution La04 (65°N summer insolation) (Laskar et al., 2004).

Figure 9. Close-up of $\delta^{18}O$ (blue) and $\delta^{13}C$ (green) of benthic *Cibicidoides pachyderma* >250 µm together with colour changes for Cores 58R, 59R and 61R. A theoretical example of a corresponding Precession-Tilt-curve is displayed to show resemblance with $\delta^{18}O$. This suggests the interference patterns of precession and obliquity in the $\delta^{18}O$. The used obliquity (grey) and precession (light blue) curves are indicated below.

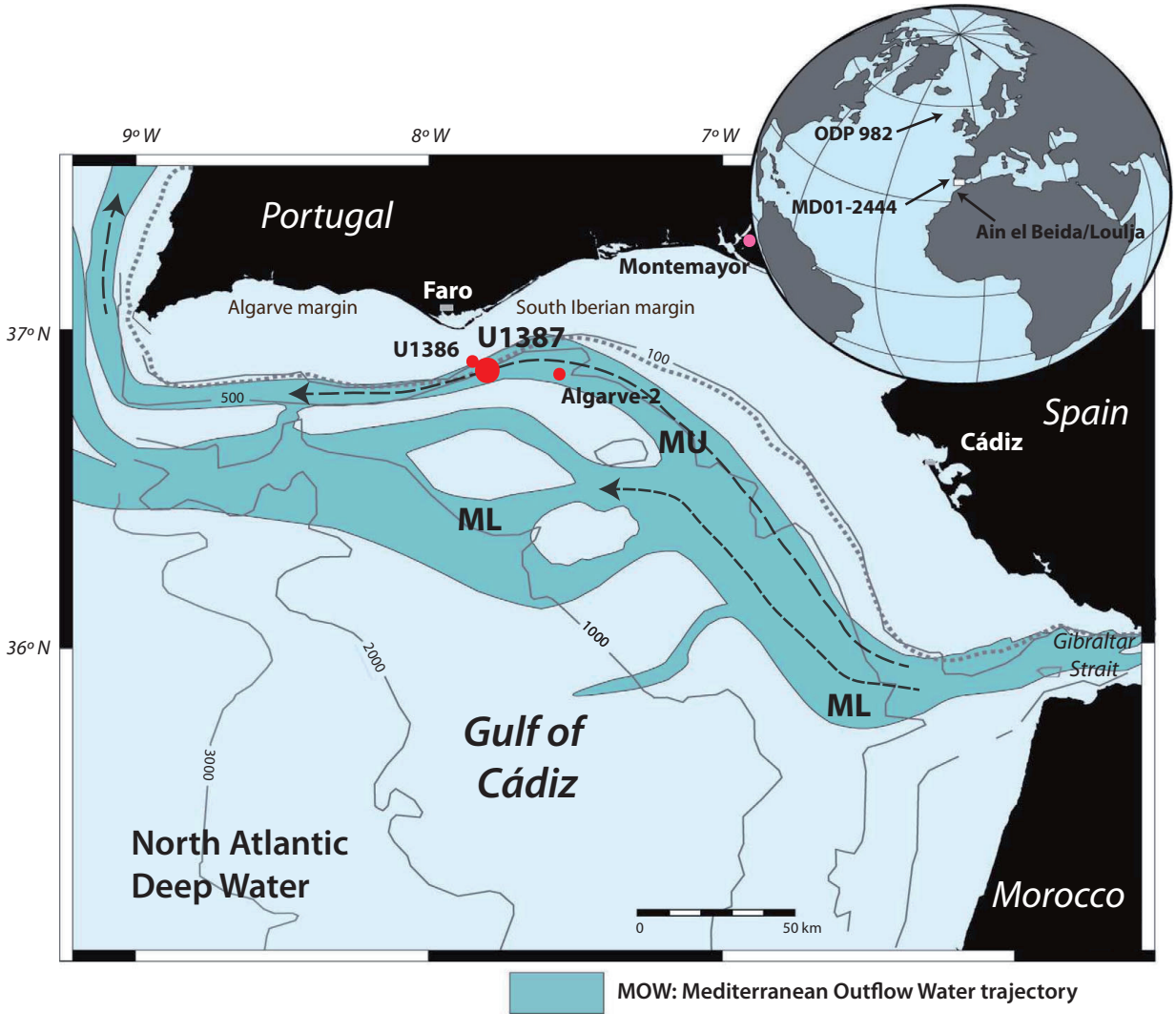
9° W
8° W
7° W
37° N
36° N
Portugal
Spain
Morocco
Faro
Montemayor
Algarve margin
South Iberian margin
U1386
U1387
Algarve-2
Cádiz
MU
ML
ML
100
500
1000
2000
3000
Gibraltar Strait
Gulf of Cádiz
North Atlantic Deep Water
0
50 km
ODP 982
MD01-2444
Ain el Beida/Loulja
MOW: Mediterranean Outflow Water trajectory
MU: Mediterranean Upper water (500-800 m)
ML: Mediterranean Lower water (1000-1400 m)

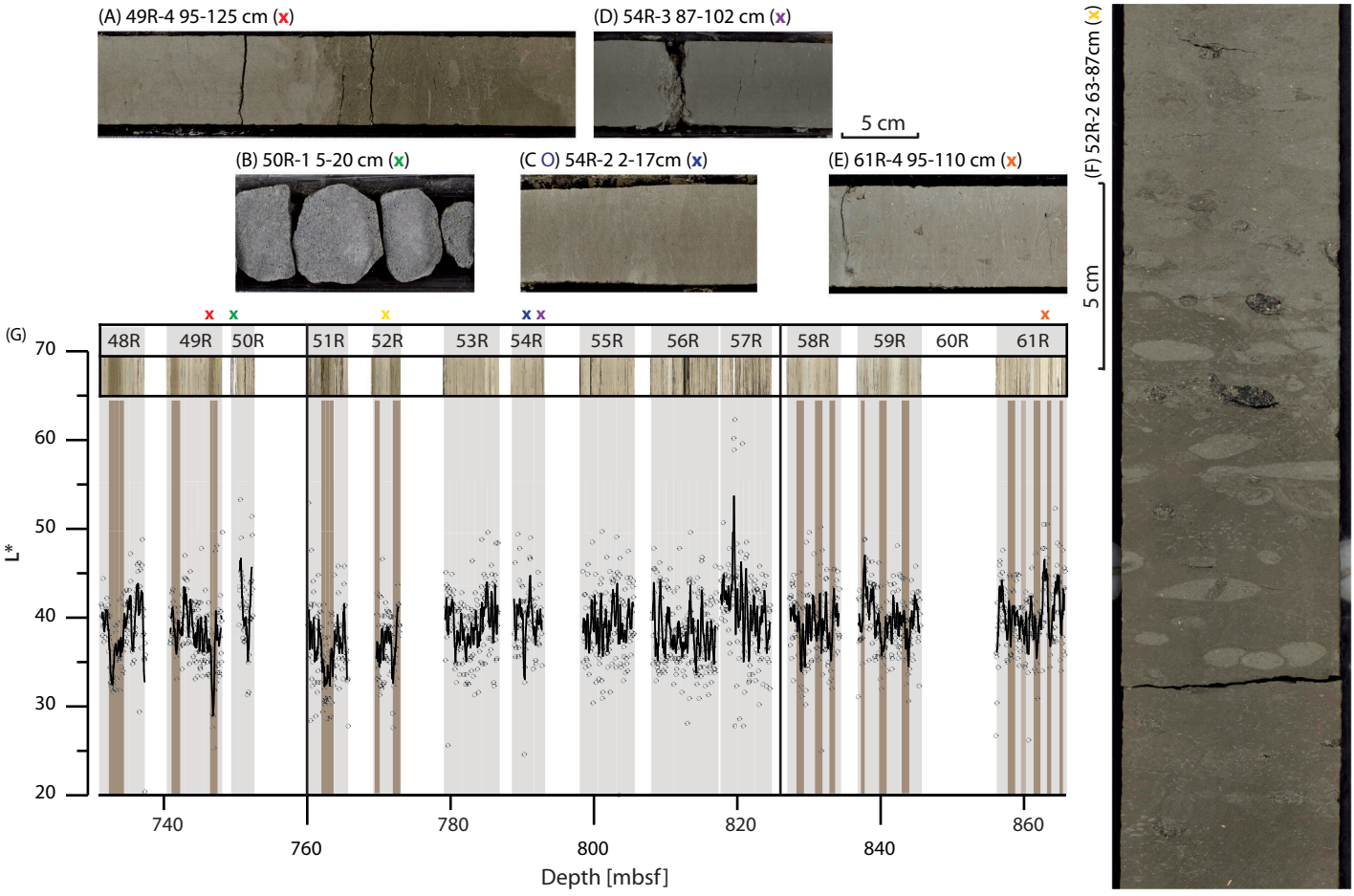
(A) 49R-4 95-125 cm (x)
(D) 54R-3 87-102 cm (x)
5 cm
(B) 50R-1 5-20 cm (x)
(C O) 54R-2 2-17cm (x)
(E) 61R-4 95-110 cm (x)
(F) 52R-2 63-87cm (x)
5 cm
(G)
48R
49R
50R
51R
52R
53R
54R
55R
56R
57R
58R
59R
60R
61R
L*
70
60
50
40
30
20
740
760
780
800
820
840
860
Depth [mbsf]

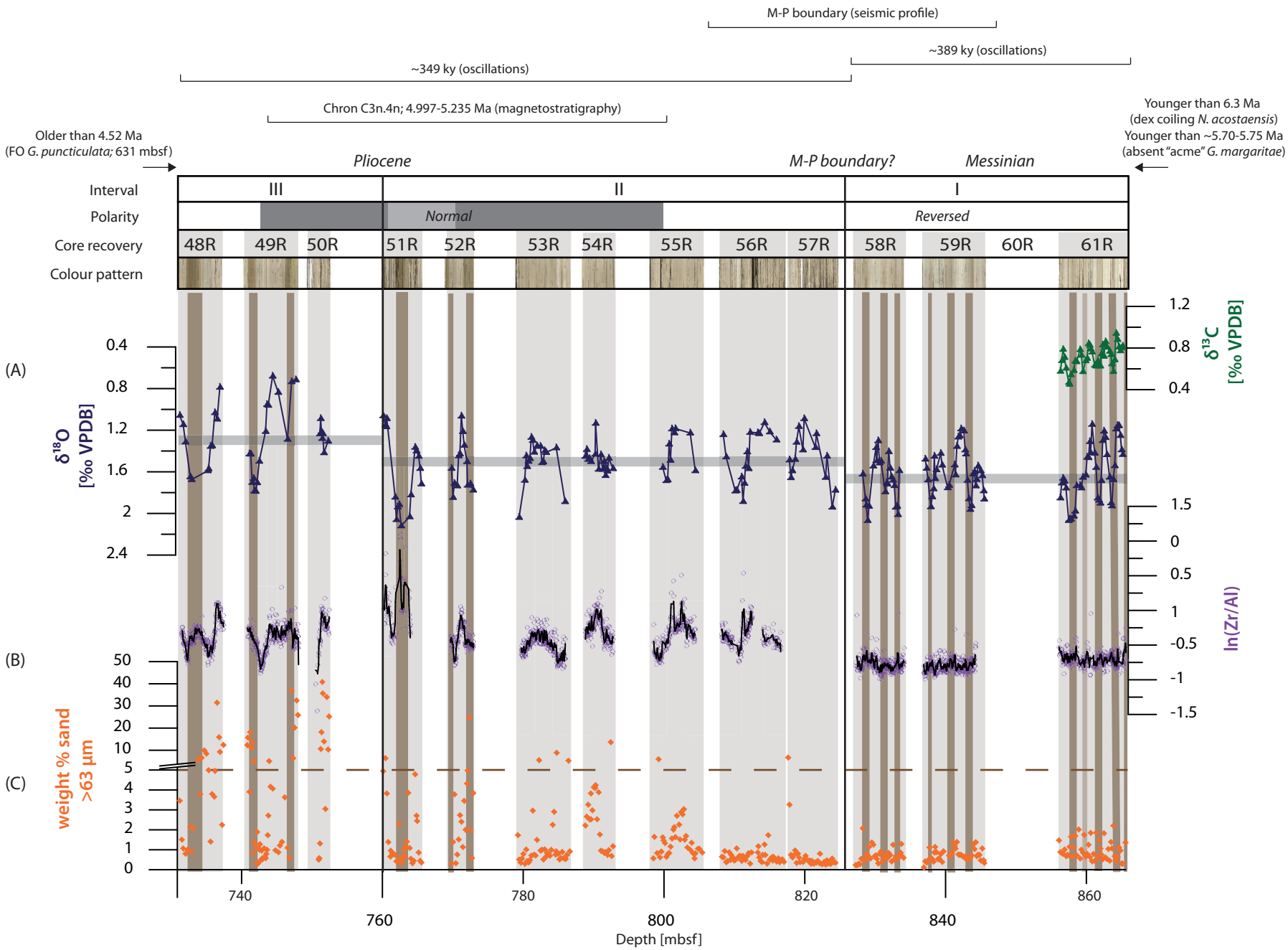
M-P boundary (seismic profile)
~389 ky (oscillations)
~349 ky (oscillations)
Chron C3n.4n; 4.997-5.235 Ma (magnetostratigraphy)
Older than 4.52 Ma
(FO G. puncticulata; 631 mbsf)
Younger than 6.3 Ma
(dex coiling N. acostaensis)
Younger than ~5.70-5.75 Ma
(absent "acme" G. margaritae)
Pliocene
M-P boundary?
Messinian
Interval
III
II
I
Polarity
Normal
Reversed
Core recovery
48R
49R
50R
51R
52R
53R
54R
55R
56R
57R
58R
59R
60R
61R
Colour pattern
(A)
δ18O [‰ VPDB]
0.4
0.8
1.2
1.6
2
2.4
δ13C [‰ VPDB]
1.2
0.8
0.4
(B)
ln(Zr/Al)
1.5
0
0.5
1
-0.5
-1
-1.5
(C)
weight % sand >63 µm
50
40
30
20
10
5
4
3
2
1
0
740
760
780
800
820
840
860
Depth [mbsf]

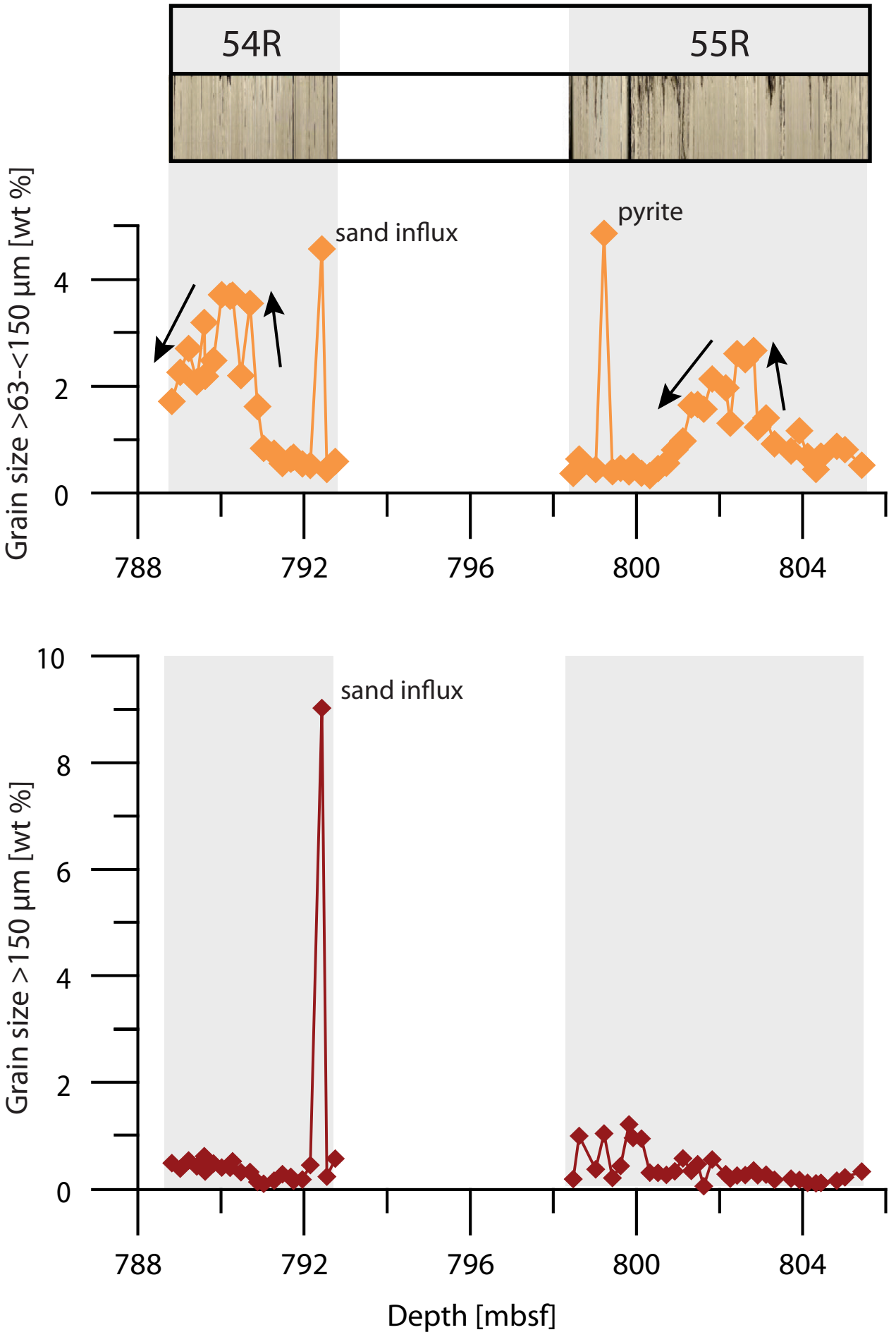
54R
55R
sand influx
pyrite
Grain size >63-<150 µm [wt %]
0
2
4
788
792
796
800
804
sand influx
Grain size >150 µm [wt %]
0
2
4
6
8
10
788
792
796
800
804
Depth [mbsf]

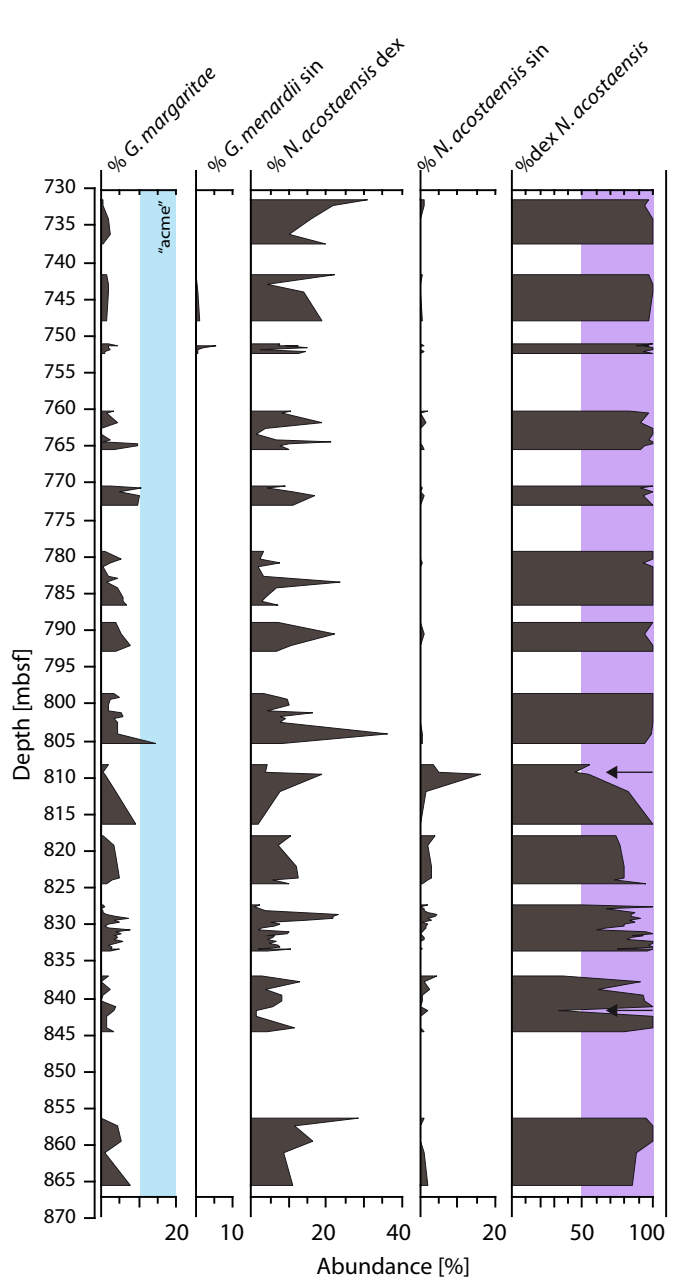
% G. margaritae
% G. menardii sin
% N. acostaensis dex
% N. acostaensis sin
%dex N. acostaensis
"acme"
Depth [mbsf]
730
735
740
745
750
755
760
765
770
775
780
785
790
795
800
805
810
815
820
825
830
835
840
845
850
855
860
865
870
20
10
20
40
20
50
100
Abundance [%]

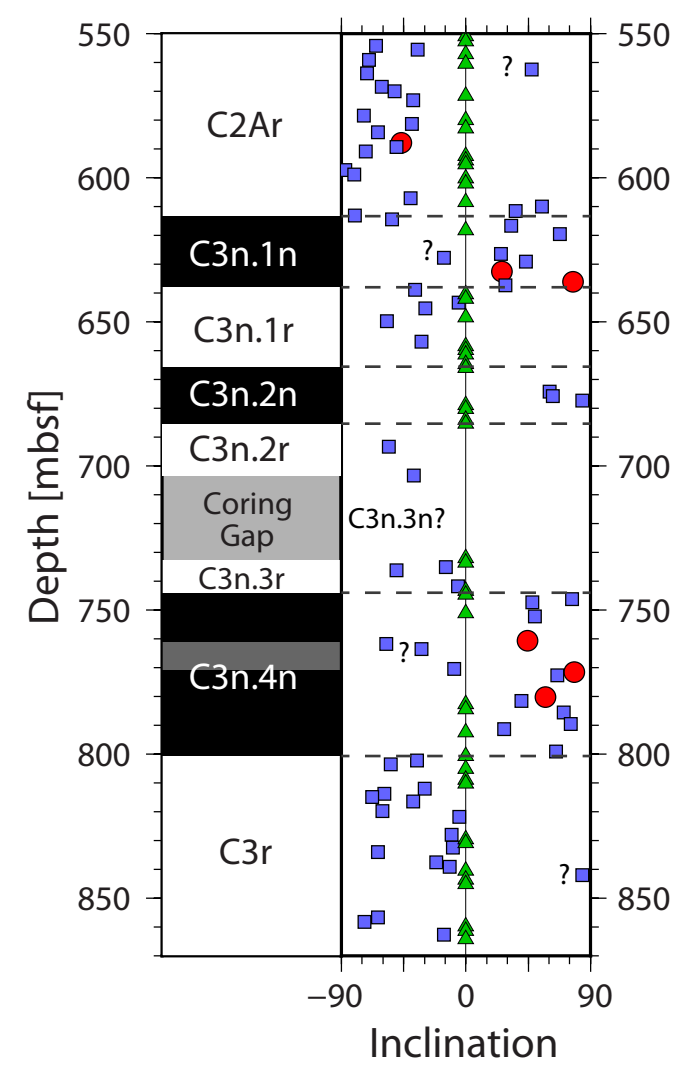
550
600
650
700
750
800
850
Depth [mbsf]
C2Ar
C3n.1n
C3n.1r
C3n.2n
C3n.2r
Coring Gap
C3n.3n?
C3n.3r
C3n.4n
C3r
?
?
?
?
–90
0
90
Inclination

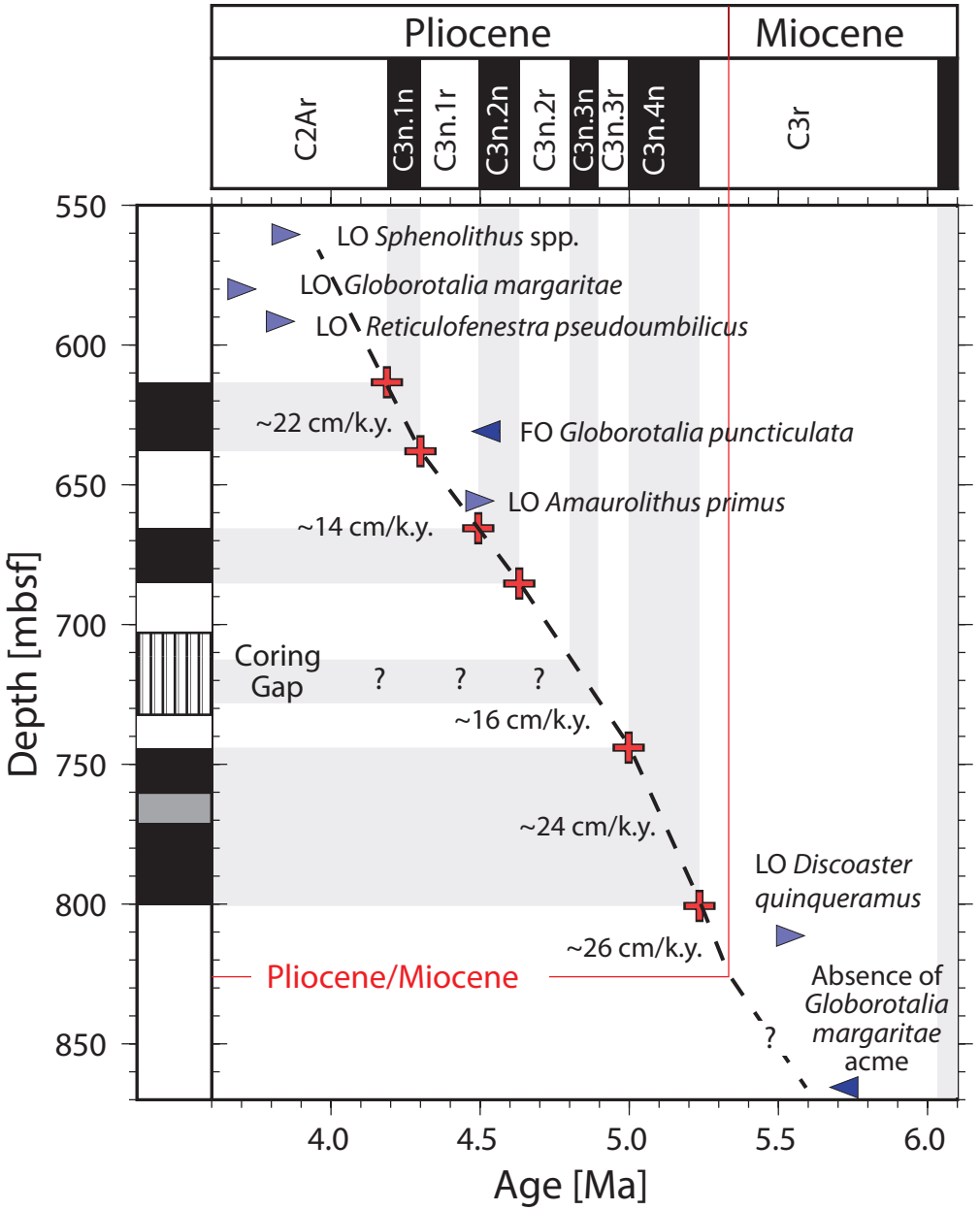
Pliocene
Miocene
C2Ar
C3n.1n
C3n.1r
C3n.2n
C3n.2r
C3n.3n
C3n.3r
C3n.4n
C3r
LO Sphenolithus spp.
LO Globorotalia margaritae
LO Reticulofenestra pseudoumbilicus
~22 cm/k.y.
FO Globorotalia puncticulata
LO Amaurolithus primus
~14 cm/k.y.
Coring Gap
? ? ?
~16 cm/k.y.
~24 cm/k.y.
LO Discoaster quinqueramus
~26 cm/k.y.
Pliocene/Miocene
Absence of Globorotalia margaritae acme
?
Depth [mbsf]
550
600
650
700
750
800
850
4.0
4.5
5.0
5.5
6.0
Age [Ma]

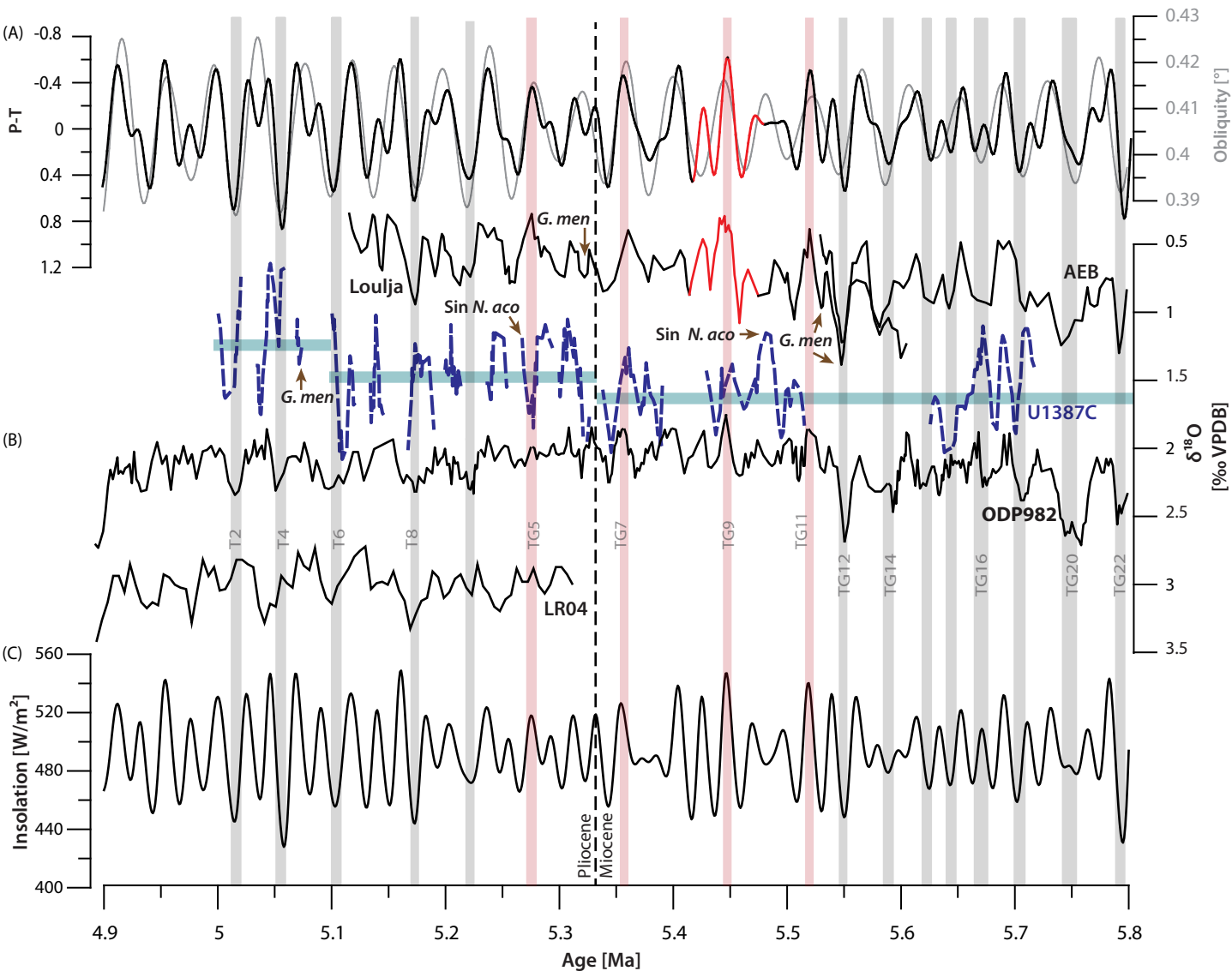
(A)
P-T
-0.8
-0.4
0
0.4
0.8
1.2
Obliquity [°]
0.43
0.42
0.41
0.4
0.39
Loulja
G. men
Sin N. aco
G. men
Sin N. aco
G. men
AEB
U1387C
(B)
ODP982
LR04
δ18O [‰ VPDB]
0.5
1
1.5
2
2.5
3
3.5
T2
T4
T6
T8
TG5
TG7
TG9
TG11
TG12
TG14
TG16
TG20
TG22
(C)
Insolation [W/m2]
560
520
480
440
400
Pliocene
Miocene
4.9
5
5.1
5.2
5.3
5.4
5.5
5.6
5.7
5.8
Age [Ma]

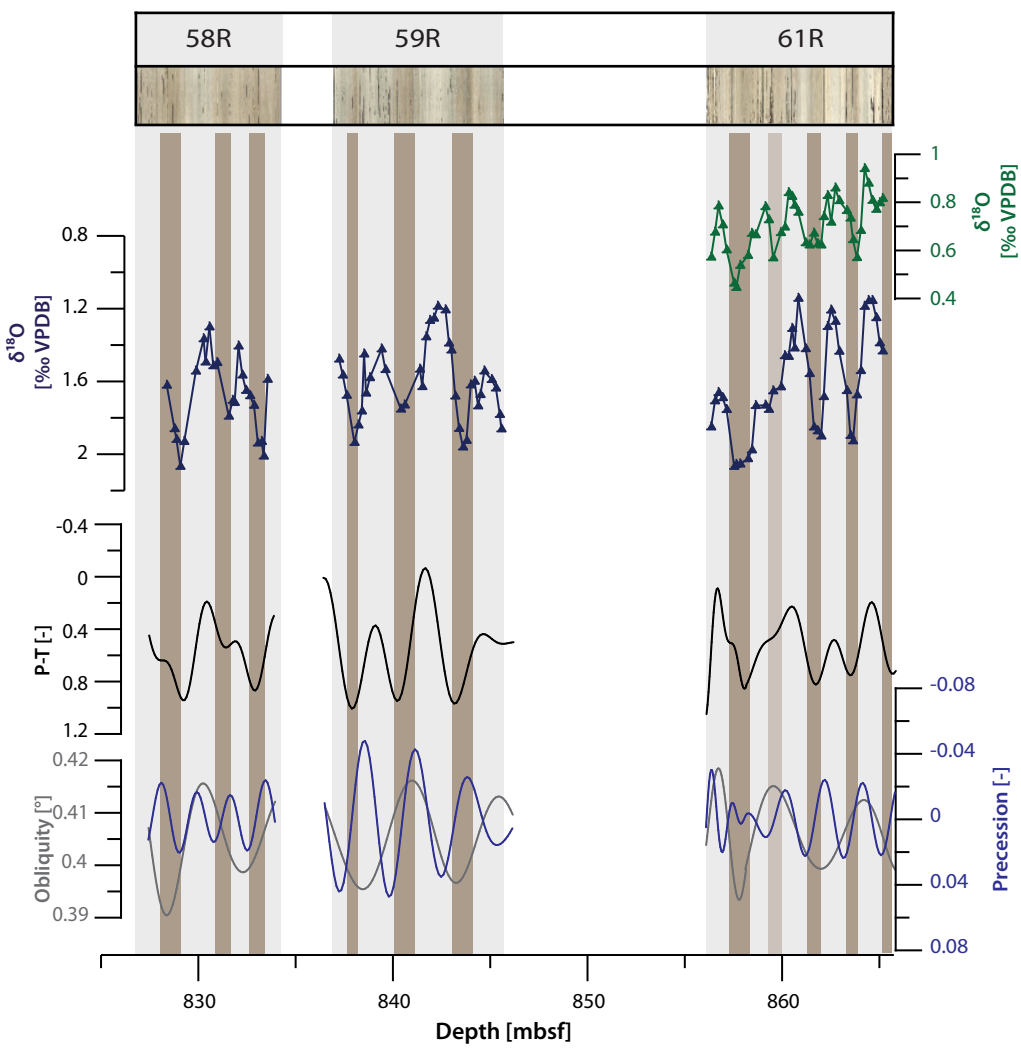
58R
59R
61R
δ18O [‰ VPDB]
0.8
1.2
1.6
2
δ18O [‰ VPDB]
1
0.8
0.6
0.4
P-T [-]
-0.4
0
0.4
0.8
1.2
Obliquity [°]
0.42
0.41
0.4
0.39
Precession [-]
-0.08
-0.04
0
0.04
0.08
830
840
850
860
Depth [mbsf]

Planktic foraminifera biohorizon	Hole U1387C depth [mbsf] Top	Bottom	Mean	Preliminary IODP report	Age Bio-event [Ma]	Reference
LO *G. margaritae*	558.9	561.89	560.4	Yes	3.85	Lourens et al., 2004
FO *G. puncticulata*	629.12	632.52	630.82	Yes	4.52	Lourens et al., 2004
Influx *G. menardii*	752.4	751.3	751.85	No	5.55, 5.51, 5.31	Krijgsman et al., 2004; Van der laan et al., 2006
Dex/sin coiling *N. acostaensis*	808.22 841.8	809.52	808.87	No	5.30, 5.32	Lourens et al., 1996; Iaccarino et al., 1999b
Acmee *G. margaritae* > 10%	Not present (below bottom of the hole)			No	5.84-5.75 5.84-5.70	Krijgsman et al., 2004; Van den Berg et al., 2015
Sinistral to dextral coiling change *N. acostaensis*	Not present (below bottom of the hole)			No	6.37	Hilgen and Krijgsman, 1999; Krijgsman et al., 2004; Sierro et al., 2001, Lourens et al., 2004

Core	Hole U1387C depth [mbsf] Top	Bottom	Length [m]	Cycles [-]	Length/cycle [m/cycle]
48R	731.2	736.91	5.71	<1	**-**
54R-57R	790.44	819.91	29.47	5.0	**5.89**
58R	828.92	832.92	4.00	2.0	2.00
59R	837.90	844.50	6.60	2.5	2.64
61R	856.68	864.42	7.74	3.0+1*	1.94
				Weighted average Interval I (58R-61R):	**2.16**